IMPAIRED LYSOSOMAL MATURATION IN MACROPHAGES UNDERLIES PATHOGENESIS IN SYSTEMIC LUPUS ERYTHEMATOSUS

Andrew Joseph Monteith

A dissertation submitted to the faculty at the University of North Carolina at Chapel Hill in partial fulfillment of the requirements for the degree of Doctor of Philosophy in the Department of Biochemistry and Biophysics in the School of Medicine.

Chapel Hill
2015

Approved by:

Barbara J. Vilen

Edward J. Collins

Ken Jacobson

M. Joseph Costello

Jean G. Cook

ABSTRACT

Andrew Joseph Monteith: Impaired lysosomal maturation in macrophages underlies pathogenesis in systemic lupus erythematosus
(Under the direction of Barbara Vilen)

Defects in clearing apoptotic debris disrupt tissue and immunological homeostasis leading to autoimmune and inflammatory diseases. We identified that macrophages from lupus-prone MRL/*lpr* mice have impaired lysosomal maturation resulting in heightened ROS production and attenuated lysosomal acidification. This diminishes their ability to degrade apoptotic debris contained within IgG-immune complexes (IgG-ICs) and promotes recycling and the accumulation of nuclear self-antigens at the membrane 72 hours after internalization. Diminished degradation of IgG-ICs prolongs the intracellular residency of nucleic acids leading to the activation of Toll-like receptors. It also promotes phagosomal membrane permeabilization allowing dsDNA and IgG to leak into the cytosol and activate AIM2 and TRIM21. Collectively, these underlying events promote the accumulation of nuclear antigens and activation innate sensors that drives IFNα production and heightened cell death. These data identify a novel defect in lysosomal maturation that provides a mechanism for the chronic activation of intracellular innate sensors in systemic lupus erythematosus.

Current therapeutics either broadly suppresses the immune system or target one pathogenic factor in SLE (BAFF, IFNα, B cells). Therefore, identifying the molecular mechanism preventing lysosomal maturation in lupus-prone macrophages could provide a targeted therapeutic addressing multiple SLE pathologies. We identified that heightened mTOR activation (mTORC1 and mTORC2) and chronic localization to the cell membrane impairs

lysosomal maturation and underlies the accumulation of IgG-ICs on the membrane. Furthermore treatment with Torin1 and not Rapamycin restored degradation of IgG-ICs implicating that mTORC2 activity contributed to impaired lysosome maturation. In B6 MFs we found that regulation of the activity of mTORC2 allows cofilin to depolymerize actin filaments following phagocytic cup assembly. Actin depolymerization initiated a localized caspase cascade that lead to the activation of caspase-1 in an inflammasome-independent manner. Caspase-1 then cleaved Rab39a on the membrane of phagosomes containing IgG-ICs; a necessary step for lysosomal maturation. In lupus-prone MFs, heightened mTORC2 activity phosphorylates cofilin, which prevents actin depolymerization and the caspase cascade, thus leaving Rab39a uncleaved. As a result, the lysosome is unable to mature and degrade the phagocytosed IgG-ICs. These findings identify a novel signaling pathway regulating lysosomal maturation and an underlying defect in basic cellular function that can lead to immunological activation.

ACKNOWLEDGMENTS

Chapter 2: We would like to thank Drs. Roland Tisch and Nick Spidale (University of N. Carolina-Chapel Hill) for NOD mice, Dr. Gary Gilkeson (Medical University of South Carolina) for NZM2410 mice, Dr. Christophe Benoist (Harvard Medical School) for K/BxN mice, Drs. Edward Miao and Bill Goldman (University of N. Carolina-Chapel Hill) for the GFP-*E. coli* and B6/GFP mice. We also thank the Flow Cytometry Core (NCI P30CA016086), the Microscopy Services Laboratory (CA 16086-26) for their support, and Robert Currin at the UNC Olympus Center for assistance with 2-photon imaging. This work was supported by NIH R01AI070984, NIH R21AI105613, NIH R21AR064951 and the Alliance for Lupus Research. A.J.M. was supported by 5T32AI07273. The authors declare no competing financial interests.

Chapter 3: We would like to thank Drs. Edward Miao and Manira Rayamajhi (University of N. Carolina-Chapel Hill) for the Caspase-$1^{-/-}$Caspase-$11^{-/-}$/B6, Caspase-$11^{-/-}$/B6, and $Asc^{-/-}$/B6 mice, v-Myc MFs, and Rab39a plasmids. We would like to thank Drs. James Bear and Jeremy Rotty for supplying phalloidin-Alexa 568, jasplakinolide, and LimKi 3. We would like to thank Dr. Tony Richardson and Lance Thurlow for supplying rapamycin. We also thank the Flow Cytometry Core (NCI P30CA016086) and the Microscopy Services Laboratory (CA 16086-26) for their support. This work was supported by NIH R01AI070984, NIH R21AI105613, NIH R21AR064951 and the Alliance for Lupus Research. A.J.M. was supported by 5T32AI07273. The authors declare no competing financial interests.

TABLE OF CONTENTS

LIST OF FIGURES

LIST OF ABBREVIATIONS

AIM2	absent in melanoma 2
AP	adaptor protein
APC	antigen presenting cell
ASC	apoptosis-associated speck-like protein
ATP	adenosine triphosphate
BAFF	B cell activating factor
B6	C57BL/6
BCR	B cell receptor
CD	cluster of differentiation
CNS	central nervous system
CRP	C-reactive protein
DC	dendritic cell
dsDNA	double stranded deoxyribonucleic acid
E. coli-IC	*Escherichia coli* bound by IgG autoantibodies forming immune complexes
ESCRT	endosomal sorting complexes required for transport
FcγR	Fc-γ receptor
GTP	guanosine triphosphate
IFN	interferon
IC	immune complex
IgG	immunoglobulin G
IgG-IC	apoptotic debris bound by IgG autoantibodies forming immune complexes
IRAK	interleukin-1 receptor-associated kinase

IRF	interferon regulatory factor
ITAM	immunoreceptor tyrosine-based activation motif
ITIM	immunoreceptor tyrosine-based inhibitory motif
LAMP	lysosomal-associated membrane protein
LC3	light chain 3
MF	macrophage
mTORC1	mammalian target of rapamycin complex 1
MyD88	myeloid differentiation primary response gene 88
NETs	neutrophil extracellular traps
NF-κB	nuclear factor κ-light-chain-enhancer of activated B cells
NLRP	NOD-like receptor protein
Nox2	NADPH oxidase 2
PI3K	phosphatidylinositol-4,5-bisphophate 3-kinase
PTPN22	protein tyrosine phosphatase, non-receptor type 22
ROS	reactive oxygen species
SLE	systemic lupus erythematosus
Sm	Smith antigen
STAT	signal transducer and activator of transcription protein
STING	stimulator of interferon genes
TCR	T cell receptor
TIRF	total internal reflection fluorescence
TLR	Toll-like receptor
TNFAIP3	tumor necrosis factor alpha-induced protein 3

TNP	2,4,6-trinitrophenol
TNP-IC	TNP bound by IgG autoantibodies forming immune complexes
TREX1	three prime repair exonuclease 1
TRIM21	tripartite motif-containing protein 21
UNC93B1	Unc-93 homolog B1
V-ATPase	vacuolar-type H^+-ATPase

CHAPTER 1: Introduction

In a healthy individual the immune system is equipped with the tools to mount strong pro-inflammatory responses that are critical in combating infection from microorganisms (bacteria, viruses, parasites) while also limiting immune responses against self-antigens. When tolerance mechanisms fail, the immune system can respond to self-antigens resulting in autoimmunity. Systemic lupus erythematosus (SLE) is a multi-system autoimmune disease with genetic and environmental components that promote the activation of the immune system against nuclear self-antigens (ie: dsDNA, histones, ribonucleoproteins) This results in tissue-damaging inflammation that affects multiple organs (skin, joints, heart, CNS, kidney) (*1*). The systemic nature of SLE leads to multiple different clinical presentations, making it difficult to diagnose and determine an underlying mechanism for disease.

Observational studies have long associated SLE with the accumulation of apoptotic debris and immune complexes (ICs) containing apoptotic debris (IgG-ICs) in SLE (*2-5*). The accumulation of apoptotic debris has been attributed to impaired clearance of apoptotic bodies rather than increased rates of apoptosis (*6*). It has been demonstrated that human SLE patients have polymorphisms in, and decreased expression of, scavenger receptors, increased expression of FcγRs, and deficiencies in complement (*7-12*), though whether macrophages (MFs) harbor intrinsic defects that contribute to impaired clearance is highly debated (*13, 14*). Murine models lacking MFGE8 and the complement proteins, opsonins thought to be important to the clearance of apoptotic bodies, have impaired clearance of apoptotic bodies and spontaneously develop autoimmunity (*15, 16*). Furthermore, the opsonization of apoptotic bodies with autoreactive IgG

has been demonstrated to impair phagocytic uptake by MFs (*17*). Interestingly, not all defects in apoptotic cell clearance seem to promote autoimmunity as murine models lacking mannose binding lectin and CD14 fail to develop autoimmunity despite having increased apoptotic debris in the tissues (*18, 19*). This suggests that accumulation of apoptotic debris alone is not sufficient in promoting autoimmunity and that the manner in which apoptotic debris is cleared may provide a critical downstream immunomodulatory signal that can either prevent or promote autoimmunity.

Fcγ receptors (FcγRs) clear of apoptotic debris, tolerize B cells to self-antigens, and transmit downstream immunomodulatory signals that control cellular activation. FcγRs recognize the Fc portion of the antibodies that constitute the IgG-ICs. Upon ligation, FcγRs on dendritic cells (DCs) and MFs promotes phagocytosis and signal transduction. There are two types of FcγRs: immunoreceptor tyrosine-based activation motif (ITAM) -containing which activate the cell and immunoreceptor tyrosine-based inhibitory motif (ITIM) -containing which repress ITAM signaling. Phagocytosis through ITAM-containing FcγRs (human: FcγRI/IIa/IIc/IIIa; mice: FcγRI/III/IV) recruit Syk, leading to the activation of the PI3k pathway (*20-22*) and trafficking of phagocytosed IgG-ICs to lysosomal structures for degradation (*23, 24*). Interestingly, polymorphisms that decrease the binding to IgG to human FcγRIIa (R/H131) and FcγRIIIa (158V/F) have been associated with lupus nephritis and are thought to diminish clearance of apoptotic debris (*25*). In contrast to phagocytosis through ITAM-containing FcγRs, the ITIM-containing FcγRIIb represses ITAM-containing FcγRs by recruiting SHIP1 to dephosphorylate $PI(3,4,5)P_3$ at the cellular membrane limiting, downstream signal propagation (*26, 27*). Further, instead of trafficking IgG-ICs to lysosomes, FcγRIIb traffics IgG-ICs to recycling endosomes where they are re-expressed at the membrane to tolerize B cells (*23*). Mice

lacking FcγRIIb develop lupus-like disease (*28*), while promotor polymorphisms reducing the expression of FcγRIIb has been associated with murine and human SLE (*29, 30*). Strangely, complete loss of FcγR on the lupus-prone MRL/*lpr* background (FcγR$^{-/-}$MRL/*lpr*) had no effect on disease pathology (*31*), while loss of FcγRs in lupus-prone NZB/W F1 (FcγR$^{-/-}$NZB/W F1) mice have diminished disease (*32*). It was later discovered that FcγR deficient mice maintain a partially functional FcγRI complicating the previous interpretations (*33*). Despite this finding, it's interesting that different murine models of SLE have varying dependencies on FcγRs, although how FcγRs are specifically contributing to disease remains unknown.

Of the surface FcγRs, FcγRI has the highest affinity for IgG (10^{-8} M compared to 10^{-5}-10^{-7} M) (*34*) because of the third extracellular IgG-like domain (*35*). Not only has this receptor been demonstrated to play an important role in protection against bacterial infections, but it also exacerbates multiple autoimmune diseases (*36, 37*). Upon ligation, FcγRI internalizes large ICs through actin-dependent phagocytosis and small ICs through clatherin mediated endocytosis (*38*). This is dependent on the relative levels of receptor cross-linking and the competition between PI3k and Cbl for binding to Syk (*38*). During endocytosis, Cbl outcompetes PI3k and poly-ubiquitinates Syk leading to its degradation and mono-ubiquitinates FcγRI, targeting the forming endosome for lysosomal degradation (*38, 39*). In contrast, when PI3k outcompetes Cbl, Syk remains phosphorylated and promotes the actin cup rearrangements integral to phagocytosis (*38, 40, 41*). Although, there have been many studies in SLE implicating intrinsic defects in the phagocytosis of latex beads, apoptotic cells, IgG-ICs, bacteria, and yeast (*6, 8, 42-44*), no underlying mechanism has been identified.

Regardless of the method of internalization, phagosomes and endosomes fuse to form an early phagosome (*45*). The maturation status of the phagosome is controlled by two sets of

proteins: ESCRT complexes and Rab GTPases. Although the exact function of ESCRT complexes are still debated, their association with the phagosome is critical to maturation and lysosomal degradation (*46*). ESCRT-0 recognizes mono-ubiquitinated cargo at the membrane and facilitates the initial sorting of the phagosome (*47*). This allows the ESCRT-I and -II complexes to associate with the phagosome, which also contain ubiquitin binding domains (*48, 49*). The recruitment of ESCRT-I and -II forms the nexus that bridges ubiquitinated cargo to the ESCRT-III complex, promoting the trafficking of the phagosome to lysosomal structures (*50*). While mono-ubiquitination is critical for the association of ESCRT complexes, PIP_3 is critical for the Rab proteins to associate with the vesicle. Rab5 associates with the early phagosome via PIP_3 although inhibiting PI3k activity does not preclude Rab5 recruitment (*51-53*). As the phagosome matures Rab5 is exchanged for Rab7 (*53-56*), an event thought to be mediated by Rab22a (*57*). Rab7 recruits effector proteins that promote the association of the maturing phagosome with microtubules driving the phagosome towards lysosomal compartments (*58*). Interestingly, recruitment of Rab7 is insufficient to induce phagosome maturation and lysosomal degradation (*53*), suggesting that the order of recruitment is critical to phagosomal maturation. Elevated Rab4 (promotes recycling endosomes) and Rab5 have been found in CD4 T cells from SLE patients (*59*), though their effect on disease pathology is unclear.

Concurrent with the recruitment of ESCRT complexes and Rab GTPases to the cytosolic side of the phagosome, the lumen of the phagosome evolves throughout its maturation. The assembly of the NADPH oxidase (Nox2) on the early phagosomal membrane is a major antimicrobial effector as it produces high levels of superoxide (herein referred to as ROS) within the phagosomal lumen (respiratory burst). Heightened ROS production by granulocytes and monocytes has been observed in SLE (*60*), though the role of ROS in disease progression is

unknown. One attractive candidate for the production of ROS and source of autoantigen is the formation of neutrophil extracellular traps (NETs) by neutrophils (*61, 62*), mast cells (*63*), and eosinophils (*64*) in which DNA coated with antimicrobial proteins are extruded into the extracellular environment in a Nox2-dependent form of cell death termed "NETosis". It has been demonstrated that delivery of NET DNA to plasmacytoid dendritic cells (pDCs) results in type 1 interferon (IFN) production in a toll-like receptor (TLR) dependent manner (*65, 66*). Observational studies also have found DNA projections consistent with NET formation in the glomeruli of SLE patients (*67, 68*). While these results were promising, Nox2 deficiency in lupus-prone mice had significantly exacerbated disease with severe golerulonephritis (*69*), while earlier anecdotal studies linked Nox2 deficiencies with increased SLE in humans (*70-72*). This suggests that even though heightened NET formation may occur in SLE, its role may actually be protective and playing a role in reducing pathology. This suggests that the heightened ROS levels seen as pathologic in SLE may be NET-independent and connected to the respiratory burst of non-NETosing cells.

Termination of the respiratory burst must occur prior to phagosomal fusion with a lysosome to allow proper acidification of the phagolysosome (*73*). Lysosomes contain proteolytic enzymes (proteases, DNases, RNases, Lipases, etc.) that require a low pH (pH≤4) to properly activate and degrade the phagocytosed cargo (*74, 75*). To limit the lysosomal degradation of antigens, DCs utilize ROS production during the respiratory burst to alkalize the phagolysosome to maintain efficient antigen crosspresentation to T cells (*76-78*). Conversely, MFs are specialized in proteolytically degrading internalized cargo and possess a capacity of lysosomal proteolysis that is 20- to 60-fold higher than DCs (*79-81*). As a result, a prolonged respiratory burst has no alkalizing effect on lysosomal pH, but instead inhibits cysteine

cathepsins by modulating the local redox environment, which limits degradation (*82*). Interestingly, observational studies in SLE have found impairment of lysosomal acidification (*43, 83*), impaired DNase II activity (*84, 85*), and LAMP proteins localizing to the cell membrane (*86, 87*), which could implicate lysosome function in disease progression. While this could explain the accumulation of IgG-ICs associated with SLE, there has been no mechanism connecting lysosome dysfunction to SLE pathology and as a result there's no consensus in the field whether immune cells harbor defects in phagocytosis, lysosomal degradation, or both.

Innate receptor activation has long been attributed with SLE pathogenesis, although the source of nuclear antigen and how the receptors are activated remains unknown. The autoimmune response against nucleic acids depends on TLR7 and TLR9, and their correlation with SLE pathology has been highly studied (*88-92*). TLR7 and TLR9 reside in the endoplasmic reticulum (ER) in the pro-form until UNC93B1 shuttles the TLRs to the Golgi (*93-95*). TLRs are differentially trafficked from the Golgi, where TLR9 traffics to the membrane prior to arriving at the phagolysosome in an AP-2 dependent mechanism, while TLR7 traffics directly to the phagolysosome in an AP-4 dependent mechanism (*96*). Upon arrival at the phagolysosome, TLR7 and TLR9 become proteolytically cleaved, allowing them to activate upon ligation to ssRNA (TLR7) and dsDNA (TLR9), although the exact mechanism for TLR7 cleavage is unknown (*94, 97*). Interestingly, murine models expressing heightened TLR7 causes development of SLE-like disease (*98-100*). Furthermore MRL/*lpr* lacking TLR9 had exacerbated disease, while TLR7-deficient mice had ameliorated disease (*88*). This suggests that TLR7 and TLR9 might have contrasting roles in SLE, despite both being activated by nuclear antigens.

There is a subset of innate sensors that are free in the cytosol and activation of these cytosolic sensors by nuclear antigens has also been implicated in SLE. The Nba2 locus is a major contributor to disease susceptibility in the NZB/W F1 murine model of lupus and contains 2 cytosolic sensors that recognize dsDNA (p202 and Aim2). NZB/W F1 mice have heightened expression of p202 (*101*) which binds to dsDNA and inhibits Aim2 inflammasome formation (*102*). Furthermore, decreased Aim2 expression promotes decreased FcγRIIb expression, increased p202 expression, and heightened IFN production (*103*). Overall, p202 prevents Aim2-mediated pyroptosis and allows other cytosolic sensors to recognize nucleic acids and drive type I IFN production (*104*). Identifying these other cytosolic sensors to nuclear antigen has proved to be difficult as studies in SLE patients and murine models of SLE have produced contradicting reports on the roles of NLRP3/NLRP1 (*105-108*) and STING (*109-112*) in autoimmunity. The cytosolic sensor TRIM21 is the highest affinity Fc-receptor (*113*) and is responsible for recognizing opsonized pathogens in the cytosol and promoting their degradation and type 1 IFN production (*114, 115*). In autoimmunity, a high frequency of patients across multiple autoimmune diseases have autoantibodies against TRIM21 with the highest frequency being SLE and Sjögren's syndrome (*116-118*). Furthermore, a polymorphism in TRIM21 (*119*) and heightened expression of TRIM21 (*120*) and its regulated genes (*120, 121*) has been identified in SLE patients.

While a role for cytosolic sensors in autoimmunity has become apparent, how autoantigens reach the cytosol is unknown. The P2X7 receptor (P2X7R) is an ATP-gated cell membrane receptor connected to the secretion of proinflammatory cytokines (*122-124*), cell death (*125-127*). Further, its under-expression in T cells has been connected to murine models of lupus (*128*). P2X7R is unique because in the presence of high levels of ATP, P2X7R forms a

pore in the cell membrane that allows large organic molecules to enter the cytoplasm (*129*). This brings up the possibility that P2X7R may facilitate entry of extracellular autoantigens into the cytosol. Interestingly, the *P2X7R* gene is located in an SLE susceptibility locus (SLEB4) (*130*) and polymorphisms in P2X7R have been identified with SLE (*131*). A mechanisms linking membrane permeabilization, cytosolic sensor activation, and autoantigens has yet to be elucidated in autoimmunity.

Herein we report that MRL/*lpr* MFs have impaired lysosomal maturation that prevents the degradation of phagocytosed IgG-ICs (Fig. 1, **1**). This defect is not unique to IgG-ICs as *E. coli* opsonized with IgG fails to be degraded. Also, the defect is not ubiquitous to all internalized cargo because TNP-ICs (2,4,6-trynitrophenol opsonized by IgG) are degraded. As a result, intact IgG-ICs recycle to the cell membrane and accumulate on the cell surface 72 hours after being phagocytosed (Fig. 1, **2**). The prolonged residency of nuclear antigen in the phagolysosome allows for the chronic activation of intracellular TLRs (Fig. 1, **3**), and permeabilization of the phagolysosomal membrane (Fig. 1, **4**) results in dsDNA and IgG to gain access to the cytosol and activate Aim2 (Fig. 1, **5**) and TRIM21 (Fig. 1, **6**). This heightens cell death and promotes the secretion of IFNα in lupus-prone MRL/*lpr* MFs.

The impaired lysosomal maturation in MRL/*lpr* MFs is the result of active mTOR and its mislocalization at the cell membrane (Fig. 2, **1**) as treatment with Torin1 (mTORC1/C2 inhibitor) removes mTOR from the membrane and allows for lysosomal acidification and degradation of IgG-ICs (Fig. 2, **2**). Impairing mTORC1 with Rapamycin is not sufficient in restoring lysosomal degradation suggesting a role for mTORC2. The activation of mTORC2 drives cofilin phosphorylation which prevents the depolymerization of actin following phagocytic cup assembly (Fig. 2, **3**). Actin depolymerization initiates a localized caspase

cascade (Fig. 2, **4**) that allows activated caspase-1 to cleave Rab39a (Fig. 2, **5**); a necessary step for lysosomal maturation. MRL/*lpr* MFs fail to efficiently depolymerize actin and recruit caspase-11 on f-actin (Fig. 2, **6**) and preventing caspase-1 mediated cleavage of Rab39 (Fig. 2, **7**).

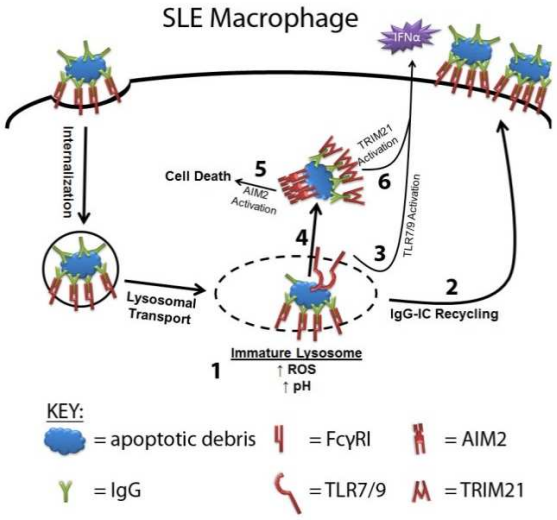

Figure 1. Lupus-prone MFs fail to mature the lysosome and as a result activate intracellular sensors.

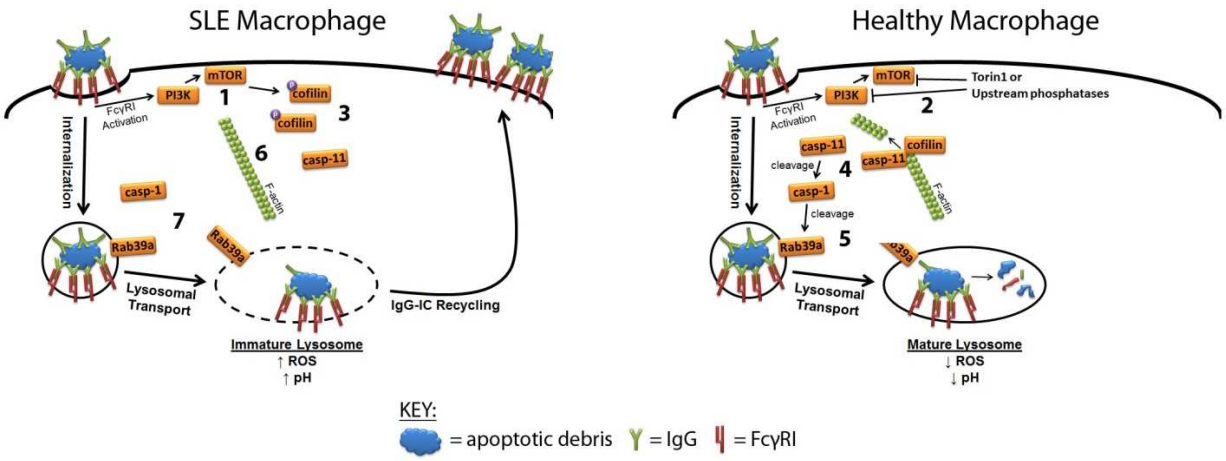

Figure 2. Signaling pathway regulating Rab39a mediated lysosomal maturation in lupus-prone and healthy MFs.

CHAPTER 2: Defects in lysosomal maturation facilitate the activation of innate sensors in systemic lupus erythematosus

Defects in clearing apoptotic debris disrupt tissue and immunological homeostasis leading to autoimmune and inflammatory diseases. Herein we report that macrophages from lupus-prone MRL/*lpr* mice have impaired lysosomal maturation resulting in heightened ROS production and attenuated lysosomal acidification. This diminishes their ability to degrade apoptotic debris contained within IgG-immune complexes (IgG-ICs) and promotes recycling and the accumulation of nuclear self-antigens at the membrane 72 hours after internalization. Diminished degradation of IgG-ICs prolongs the intracellular residency of nucleic acids leading to the activation of Toll-like receptors. It also promotes phagosomal membrane permeabilization allowing dsDNA and IgG to leak into the cytosol and activate AIM2 and TRIM21. Collectively, these underlying events promote the accumulation of nuclear antigens and activation innate sensors that drives IFNα production and heightened cell death. These data identify a novel defect in lysosomal maturation that provides a mechanism for the chronic activation of intracellular innate sensors in systemic lupus erythematosus.

Introduction

The disposal of apoptotic debris is initiated by membrane changes that facilitate the binding of IgM antibodies, acute phase proteins (CRP), and other serum opsonins to enhance phagocytosis (*132, 133*). The disposal of apoptotic debris is crucial to immune homeostasis as the accumulation of apoptotic debris (*2-4*) and the formation of immune complexes (ICs) (*5*) have long been associated with systemic lupus erythematosus (SLE). Similarly, impaired

clearance of apoptotic bodies in mice lacking scavenger receptors and complement proteins induces spontaneous autoimmunity (*15, 16*). The idea that accumulated apoptotic bodies contributes to SLE is further supported in human studies describing polymorphisms or decreased expression of scavenger receptor, increased expression of FcγRs, or deficiencies in complement (*7-12*). Despite these findings, it remains unclear whether macrophages harbor intrinsic defects that contribute to impaired clearance (*13, 14*).

Apoptotic debris bound by IgG autoantibodies forms immune complexes (henceforth referred to as IgG-ICs) that heighten autoantibody production by chronically stimulating autoreactive B cell receptors (BCRs) and/or toll-like receptors (TLRs) upon delivery of nucleic acids to the endosome (*89, 92*). In addition, the binding of IgG-ICs to FcγRs on myeloid cells stimulates IFNα (*134*) and BAFF (*135*) secretion. In addition to stimulating surface receptors, the activation of cytosolic sensors also impacts the pathology of SLE. Polymorphisms in the cytosolic sensor to IgG (TRIM21) (*119*) and heightened expression of TRIM21 (*120*) and its regulated genes (*120, 121*) have been identified in SLE patients, while two cytosolic sensors that recognize dsDNA (p202 and AIM2) have been implicated in Type 1 IFN production in murine lupus (*101, 102*). The involvement of other cytosolic sensors including, NLRP3/NLRP1 (*105, 107*) and STING (*111, 112*) have been more controversial. Despite the mounting evidence implicating cell debris in the activation of innate sensors, a mechanism explaining how IgG-ICs gain access to the cytosol and chronically activate intracellular receptors/sensors has never been resolved.

Herein we show that lupus-prone MFs fail to fully mature lysosomes causing diminished lysosomal acidification and the inability to degrade phagocytosed IgG-ICs. As a result, intact IgG-ICs recycle back to the cell membrane promoting the accumulation of surface-bound nuclear

antigens. The prolonged residency of intracellular IgG-ICs in the phagolysosome leads to membrane permeabilization allowing dsDNA and IgG to leak into the cytosol and activate cytosolic sensors AIM2 and TRIM21. Furthermore, accumulation of undegraded nucleic acids inside the phagolysosome leads to the activation of TLR7 and TLR9. The combined activation of these signaling pathways results in heightened cell death through inflammasome formation and IFNα secretion.

Results

IgG-ICs accumulate in multiple murine models of autoimmunity

The accumulation of apoptotic debris has been identified in autoimmune diseases other than SLE, including apoptotic beta-cells in diabetes (*136*), and apoptotic synoviocytes in rheumatoid arthritis (*137*). Recent studies show that prior to disease, MFs from lupus-prone mice (MRL/*lpr* and NZM2410) accumulate high levels of FcγR-bound IgG-ICs (Fig. 1A-B) (*37*). Similarly, SLE patients experiencing active disease accumulate nuclear antigens on peripheral blood mononuclear cells (*37*). Therefore, we wanted to assess whether accumulation of IgG-ICs occurs in other autoimmune models by quantifying the levels of surface IgG and nuclear antigen on MFs from murine models of diabetes (NOD) and rheumatoid arthritis (K/BxN). We found that the levels of surface IgG on MFs from NOD and K/BxN mice were elevated (Fig. 1B), and showed a punctate staining pattern similar to MRL/*lpr* MFs (Fig. S1). Surface Sm levels on NOD MFs were slightly elevated, but absent on MFs from K/BxN mice. This suggests that in other autoimmune diseases MFs accumulate IgG-ICs, but the antigen bound by IgG varies. Since NOD, MRL/*lpr* and NZM2410 mice are genetically unrelated, these findings also suggest that multiple distinct genetic defects could lead to the accumulation of IgG-ICs on the cell

membrane. Therefore understanding the mechanism underlying the accumulation of IgG-ICs on the surface of MFs could elucidate a fundamental defect in autoimmunity.

Lupus-prone MFs phagocytose IgG-ICs but exhibit defective phagolysosome maturation

In SLE, the accumulation of apoptotic debris has been attributed to heightened cell death, impaired clearance, decreased complement and increased IgG levels (*2-4, 6, 17, 43, 138*). Whether lupus-prone MFs have intrinsic defects contributing to impaired clearance of apoptotic debris is debated because there are no defined mechanisms underlying diminished clearance (*13, 14*). To identify the mechanism(s) underlying the accumulation of IgG-ICs, we formed ICs using anti-nucleosome (PL2.3, IgG2a) bound to apoptotic blebs. This allows B6 and MRL/*lpr* MFs to internalize physiologically relevant IgG-ICs and a means to compare phagocytosis, intracellular trafficking, and degradation in real time. Using TIRF microscopy, we found that B6 and MRL/*lpr* MFs had comparable diffusion coefficients prior to internalization, and they internalized IgG-ICs at similar rates (Fig. 2A-B). Therefore, the accumulation of IgG-ICs on the surface of MRL/*lpr* MFs is not the result of impaired phagocytosis.

Another possible explanation for accumulation of IgG-ICs on MRL/*lpr* MFs is improper trafficking to lysosomes. However, cryo-electron microscopy showed that approximately 80% of gold-labeled IgG-ICs reached lysosomal structures in B6 and MRL/*lpr* MFs within 2 hours of phagocytosis (Fig. 2C-D). This indicates that intracellular trafficking is not impaired.

Impaired lysosomal degradation could promote membrane accumulation of IgG-ICs despite their arrival at lysosomal structures. Lysosomes contain hydrolytic enzymes that degrade cargo entering through multiple receptors including FcγRs (*24*). Activation of lysosomal enzymes requires the termination of ROS and activation of the vacuolar H^+-ATPase (V-ATPase) to achieve a pH≤5 (*82*). To determine the pH of maturing phagosomes, we introduced an

acidotropic ratiometric dye during phagocytosis of IgG-ICs. In B6 MFs, real-time two-photon microscopy identified vesicular fusion events resulting in large acidic structures (pH=4.0) (Fig. 3A-B). In MRL/*lpr* MFs, large acidic structures were rarely evident and vesicles failed to sustain a pH below 5.5. To analyze larger numbers of MFs, we used ratiometric flow cytometry to quantify the relative pH of the population. Within 30 minutes of exposure to IgG-ICs, B6 MFs reduced vesicular pH by 20% then de-acidified within 1 hour (Fig. 3C). Conversely, MRL/*lpr* MFs showed an 8% drop in pH. Concurrent with the inability to fully acidify, MRL/*lpr* MFs exhibited heightened and prolonged production of ROS (Fig. 3D). These results demonstrate that MRL/*lpr* MFs are functionally impaired in lysosomal acidification, but the impairment is not absolute as seen in lysosomal storage disorders. This is consistent with the idea that antigen processing and MHC presentation remain at least partially intact in lupus-prone mice (*139, 140*).

The impaired acidification and heightened ROS production suggests that MRL/*lpr* MFs are not properly maturing the phagolysosome, thus preventing the degradation of IgG-ICs. Maturation of the phagolysosome and autophagosome requires membrane stabilization, achieved through the recruitment of lysosome-associated membrane proteins (LAMPs) and light chain 3 (LC3). To assess whether the phagolysosome fully matures, we quantified the levels of LAMP-1 and LC3A to distinguish autophagosomes ($LC3A^+$, $LAMP\text{-}1^-$) and autophagolysosomes ($LC3A^+$, $LAMP\text{-}1^+$) from lysosomes ($LC3A^-$, $LAMP1^+$). Using confocal microscopy, we found that MRL/*lpr* MFs showed a 2-fold reduction in the association of IgG-ICs with $LC3A^-$, $LAMP\text{-}1^+$ structures (Fig. 3E-F). Since IgG-ICs arrive at lysosomal structures (Fig. 2C-D), the reduced association of LAMP-1 with vesicles containing IgG-ICs demonstrates that the impaired acidification of the lysosomes is consistent with defective phagolysosome maturation.

Lupus-prone MFs recycle IgG-ICs to the cell membrane

Damaged membrane proteins traffic to the lysosome for degradation; however, impaired degradation promotes their recycling back to the cell membrane (*141, 142*). We hypothesized that a similar mechanism might promote recycling and the accumulation of FcγR-bound IgG-ICs, since they also target lysosomal structures following activation (*24*). To test this, we co-cultured MFs with fluorophore-conjugated IgG-ICs and monitored their localization over time. Both B6 and MRL/*lpr* MFs bound similar levels of IgG-ICs, which were rapidly phagocytosed, and evident within vesicular compartments at 24 hrs (Fig. 4A-B). By 72 hours, MFs from the MRL/*lpr* mice recycled the IgG-ICs to the cell membrane, while B6 MFs retained them within the cell. The IgG-ICs appeared to remain intact and bound by FcγRs as both the antibody and apoptotic debris colocalized on the surface of the cell (Fig. S2) and the levels of surface FcγRI and IgG on MRL/*lpr* MFs increased proportionately (*37*). Overall, this supports a model wherein impaired maturation of the lysosome in MRL/*lpr* MFs diminishes degradation of IgG-ICs inducing their recycling back to the membrane.

The levels of nuclear antigen on MFs from MRL/*lpr* mice lacking FcγRI ($Fc\gamma RI^{-/-}$ MRL/*lpr*) are decreased 40% compared to cells from $Fc\gamma RI^{+/+}$/MRL/lpr mice, and they remain disease-free (*37*). This implicates the accumulation of IgG-ICs on FcγRI in SLE. Despite $Fc\gamma RI^{-/-}$MRL/*lpr* MFs binding 60% fewer IgG-ICs (Fig. 4A-B), they remain impaired in lysosomal acidification and recycle internalized IgG-ICs. This demonstrates that FcγRI is not the only receptor that recycles of IgG-ICs, and that loss of FcγRI decreases the amount of IgG-ICs that are internalized.

To assess whether recycling is unique to ICs containing apoptotic debris, we bound anti-LPS (IgG2b) to gentamicin-killed *Escherichia coli* (*E. coli*-ICs). Even though MRL/*lpr* MFs

phagocytosed fewer *E. coli*-ICs (Fig 4C), 72 hours following phagocytosis the levels of LPS on the cell surface increased 3-fold compared to those on B6 MFs (Fig. 4D). This indicates that *E. coli*-ICs also fail to be degraded by MRL/*lpr* MFs. To assess whether all ICs were recycled in MRL/*lpr* MFs, we cultured MFs with ICs formed by binding $TNP_{20}KLH$ to anti-TNP IgG2a (TNP-ICs). Surprisingly, both MRL/*lpr* and B6 MFs phagocytosed and degraded the TNP-ICs (Fig. 4E right). These data demonstrate that MRL/*lpr* MFs degrade some IgG-ICs and that recycling is not unique to ICs containing apoptotic debris.

To assess whether impaired lysosomal acidification is sufficient to induce recycling of IgG-ICs, we inhibited lysosome function in B6 MFs and assessed whether this induced IgG-ICs to recycle. Concanamycin A prevents acidification and degradation of phagocytosed cargo by specifically inhibiting the lysosomal V-ATPase. B6 MFs treated with concanamycin A recycled IgG-ICs to levels similar as MRL/*lpr* (Fig. 4F). This indicates that diminished lysosomal acidification is sufficient to promote recycling and accumulation of IgG-ICs.

Impaired lysosomal maturation permeabilizes the phagolysosomal membrane allowing dsDNA and IgG to leak into the cytosol

Studies of microbial pathogens have shown that some intracellular bacteria prevent phagosomal maturation resulting in bacterial antigens accessing the cytosol (*143, 144*). In a similar manner, impaired lysosomal maturation in MRL/*lpr* MFs might allow antigens from IgG-ICs to gain access to the cytosol and activate innate sensors. Therefore we selected two cytosolic sensors (AIM2 and TRIM21), which recognize different components from IgG-ICs (dsDNA and IgG), to determine whether the inability to mature the lysosome permeabilizes the phagolysosome allowing antigens to leak into the cytosol. To assess whether nuclear antigens gained access to the cytosol, we stimulated B6 and MRL/*lpr* MFs with IgG-ICs containing

fluorescent dsDNA. Immunoprecipitation of AIM2 from B6 and MRL/*lpr* MFs showed equal levels of AIM2 protein (Fig. 5A). Despite equal amounts of protein, MRL/*lpr* MFs had a 2.5-fold increase in the amount of dsDNA bound to AIM2 compared to B6 (Fig. 5B). In contrast, AIM2 from FcγRI$^{-/-}$MRL/*lpr* MFs bound the same level of dsDNA as B6. This suggests that although FcγRI$^{-/-}$MRL/*lpr* MFs recycle IgG-ICs (Fig. 4A-B), they leak fewer antigens into the cytosol. This might reflect decreased internalization of IgG-ICs, or that FcγR-specific signals are necessary to permeabilize the phagolysosome.

AIM2 initiates inflammasome formation by recruiting pro-caspase-1 through the linker molecule ASC. This cleaves and activates caspase-1 (*102*). To assess whether phagocytosis of IgG-ICs by MFs induces inflammasome formation, we quantified activate caspase-1, and enumerated cytosolic ASC foci (Fig. 5C-D). In the resting state, the number of MRL/*lpr* MFs containing ASC foci was higher than B6, while in FcγRI$^{-/-}$MRL/*lpr* mice they were comparable to B6. However, 4 hours after co-culture with IgG-ICs, approximately 40% of the MRL/*lpr* MFs exhibited ASC foci compared to 20% in B6 and FcγRI$^{-/-}$MRL/*lpr* MFs (Fig. 5D). This was consistent with diminished binding of dsDNA to AIM2 in B6 and FcγRI$^{-/-}$MRL/*lpr* MFs (Fig. 5A-B). In MRL/*lpr* MFs, heightened formation of ASC foci coincided with a 4.5-fold increase in activate caspase-1 compared to either B6 or FcγRI$^{-/-}$MRL/*lpr* MFs (Fig. 5E). Similarly, *ex vivo* splenic myeloid cells from MRL/*lpr* mice exhibited a 2-fold increase in active caspase-1 compared to B6 (Fig. 5F). Inflammasome formation was the consequence of lysosomal dysfunction as B6 MFs treated with concanamycin A had high levels of ASC foci and caspase-1 activation (Fig. 5D-E). Hence, impaired lysosomal degradation of IgG-ICs allows nuclear antigens to leak into the cytosol and activate innate sensors.

To corroborate the idea that diminished maturation of the lysosome promotes the permeabilization of the phagolysosome allowing antigens to leak into the cytosol, we assessed whether IgG from exogenous IgG-ICs activated TRIM21, a cytosolic sensor with high affinity for IgG (*113*). We found that 4 hours after co-culture with IgG-ICs, MRL/*lpr* MFs showed a 2-fold increase in fluorophore tagged IgG bound to TRIM21 when compared to B6 (Fig. 6A-B). The level of TRIM21-bound IgG in FcγRI$^{-/-}$MRL/*lpr* MFs was not different from B6 indicating that similar to nuclear antigen, diminished internalization of IgG-ICs reduces the amount of IgG reaching the cytosol. Similarly, co-culture of MRL/*lpr* MFs with IgG-ICs increased the levels of IgH/IgL bound by TRIM21 (Fig. 6A). We don't believe that the heightened levels of IgG bound to TRIM21 reflect the 8.8-fold increase in TRIM21 protein levels in MRL/*lpr* MFs because FcγRI$^{-/-}$MRL/*lpr* MFs also exhibited heightened levels of TRIM21 (Fig. 6A,C) and their levels of IgG bound to TRIM21 were not different than B6 (Fig. 6A-B). Thus, although elevated TRIM21 may contribute to disease pathology, it alone is insufficient, unless diminished maturation of the lysosome provides heightened levels of IgG ligand.

TRIM21 is an E3 ligase that possesses two unique functions. First, it inhibits type 1 interferon production by diminishing IRF protein levels through ubiquitination and proteasomal degradation. Second, the binding of IgG to TRIM21 stabilizes IRF proteins and activates NF-κB (*114, 115*). This heightens TLR activation and type 1 interferon production. To assess whether TRIM21 was activated, we co-cultured B6 and MRL/*lpr* MFs with IgG-ICs and quantified NF-κB activation by the nuclear translocation of p65. Resting MRL/*lpr* MFs exhibited slightly elevated nuclear p65 levels; however, after co-culture with IgG-ICs, nuclear translocation of p65 was increased 2.5-fold (Fig. 6D-E). Loss of FcγRI in MRL/*lpr* MFs restored nuclear p65 levels to those in B6. Further, p65 nuclear translocation was the consequence of failed lysosomal

acidification because concanamycin A treated B6 MFs stimulated with IgG-ICs induced a 2.5-fold increase in nuclear p65 (Fig. 6D-E). It's possible that NF-κB activation in response to IgG-ICs was the result of the apoptotic debris binding to intracellular TLRs. To assess this possibility, we co-cultured MRL/*lpr* MFs with apoptotic blebs lacking IgG. Like IgG-ICs, apoptotic blebs recycled in MRL/*lpr* MF (Fig. S3) likely because they are opsonization by C-reactive protein (CRP) and enter cells via FcγRI (*145*). Despite this, apoptotic blebs lacking IgG did not translocate p65 to the nucleus indicating that IgG was responsible for NF-κB activation (Fig. 6D-E). Thus, the inability to mature the phagolysosome allows IgG from ICs to leak into the cytosol and activate TRIM21.

The activation of TRIM21 by IgG induces poly-ubiquitination and proteasomal degradation (*146*). To assess the levels of TRIM21 activity *in vivo*, we quantified ubiquitinated TRIM21 in *ex vivo* splenic myeloid cells from B6 and MRL/*lpr* mice. We found that splenic myeloid cells from MRL/*lpr* mice had 85-fold more ubiquitinated TRIM21 compared to *ex vivo* B6 myeloid cells (Fig. 6F-G). IgG was necessary for TRIM21 ubiquitination as comparable cells from age-matched AID$^{-/-}$MRL/*lpr* mice (lack IgG) had significantly less ubiquitinated TRIM21 (13.5-fold vs 85-fold) when compared to B6 myeloid cells. Acute activation of TRIM21 stabilizes IRF3, while chronic activation increases IRF7 levels by activating NF-κB (*114, 115*). In *ex vivo* myeloid cells from MRL/*lpr* mice, we found that ubiquitinated TRIM21 was coincident with nuclear translocation of p65 and heightened levels of IRF7 protein, but not with heightened IRF3 (Fig. 6H). The finding that IRF7 protein levels are selectively increased suggests that TRIM21 activation in myeloid cells from MRL/*lpr* mice is not an acute event; but instead induced by chronic activation through IgG.

Impaired lysosomal maturation results in heightened intracellular TLR activation

Diminished lysosomal maturation allows IgG and nuclear antigens to leak into the cytosol and activate innate sensors. However, a large fraction of IgG-ICs remains inside the phagosome and is thus capable of activating TLRs. Coupled with heightened IRF7 levels from activated TRIM21 (Fig. 6H), phagosomal TLR ligands could heighten IFNα secretion through the activation of TLR7 and TLR9 (TLR7/9). To assess whether the prolonged residency of nuclear antigens within the phagolysosome activates intracellular TLRs, we quantified IRAK1 levels in MFs 24 hours after exposure to IgG-ICs. This time point was sufficient for B6 MFs to degrade the IgG-ICs, but was prior to recycling in MRL/*lpr* MFs (Fig. 4A-B). We found that MRL/*lpr* MFs exposed to IgG-ICs showed a 2.8-fold decrease in IRAK1 levels, consistent with TLR activation (Fig. 7A). Chloroquine, an acidotropic molecule that binds double and single stranded nucleotides and sterically hinders their binding to TLRs (*147*) restored IRAK1 levels supporting that TLR7/9 are activated in MFs that fail to degrade IgG-ICs. Further, impairing lysosomal acidification with concanamycin A prevents the degradation of IgG-ICs in B6 MFs (Fig. 4F) and reduced IRAK1 to levels found in MRL/*lpr* MFs (Fig. 7A). Therefore, the impaired lysosomal acidification in MRL/*lpr* MFs is sufficient to heighten TLR activation in the presence of IgG-ICs.

Formation of the TLR-MyD88-IRAK1 complex downstream of TLR7/9 promotes phosphorylation and nuclear translocation of IRF7 resulting in production of type 1 interferon (*148*). To assess whether impaired degradation of IgG-ICs promotes nuclear translocation of IRF7, we co-cultured MRL/*lpr* MFs with IgG-ICs and found they exhibited a 2-fold increase in nuclear IRF7 levels (Fig. 7B-C) that was sustained for 24 hours. IgG-ICs did not localize all IRF proteins to the nucleus as IRF3 remained cytoplasmic following exposure to IgG-ICs (Fig. 7C).

Reducing the lysosomal burden through loss of FcγRI also reduced the nuclear translocation of IRF7 in MRL/*lpr* MFs to levels comparable to B6. These findings were not an artifact of BMMFs because *ex vivo* myeloid cells from MRL/*lpr* mice also showed a 2-fold increase in nuclear IRF7, while nuclear IRF3 was not elevated (Fig. 7D). Collectively, the data support a model wherein impaired lysosomal maturation prolongs phagolysosomal residency of IgG-ICs facilitating chronic intracellular TLR activation.

The inability to degrade IgG-ICs resulted in increased levels of IRF7 and heightened intracellular TLR activation. Combined, these events could elevate IFNα secretion (*148*). To assess this, we cultured MRL/*lpr* MFs with IgG-ICs (12 and 24 hours) and found they secreted 2- and 3-fold more IFNα (Fig. 7E). The production of IFNα was a consequence of FcγRI mediated internalization because IFNα levels secreted by FcγRI$^{-/-}$MRL/*lpr* MFs were comparable to B6. This is consistent with a model wherein the accumulation of IgG-ICs in the phagolysosome of MRL/*lpr* MFs drives heightened TLR activation and IFNα secretion as a consequence of diminished lysosomal maturation.

Discussion

The mechanism underlying the accumulation of IgG-ICs in the periphery of SLE patients has been highly debated. Observational studies in SLE patients have shown that MFs have intrinsic defects in the phagocytosis of latex beads, apoptotic cells, IgG-ICs, bacteria, and yeast (*6, 8, 43, 44*). Other studies have found that phagocytosis is intact, but the ability to degrade the internalized cargo was impaired (*43, 83, 84*). We find that lupus-prone MRL/*lpr* MFs phagocytose and traffic IgG-ICs to lysosomal structures, but that the lysosomal structures are unable to mature and acidify. As a result, the IgG-ICs are not degraded and recycle back to the cell membrane. Hematopoietic cells from SLE patients have high levels of IgG and nuclear

antigens (*37*) and they express LAMP1/2 on the cell surface (*86*). This supports the idea that the lysosomal compartment has been trafficked to the membrane and is consistent with our findings showing that macrophages from lupus-prone mice accumulate high levels of nuclear antigens (Fig. 1) as a consequence of recycling undegraded IgG-ICs from the lysosome (Fig. 4). Interestingly IgG-ICs, apoptotic blebs, and *E. coli*-ICs recycled to the cell membrane while TNP-ICs were degraded. This suggests that the size or content of the cargo impairs the lysosome. Alternatively, the opsonin coating the incoming apoptotic debris could impact lysosomal maturation. Combined this could explain the variability of previous studies aimed at identifying phagocytic or lysosomal defects in SLE monocytes.

Spontaneous SLE has been linked to alterations in expression (*98*) and activation of TLR7/9 (*89, 92*), dysregulation of the cytosolic sensors p202 and AIM2 (*101, 102*), and polymorphisms (*119*) and heightened expression in TRIM21 (*120*). We now define that defective degradation of FcγR-bound cargo in the lysosome is a critical upstream event that overburdens phagolysosome. The prolonged intracellular residency of IgG-ICs promotes the activation of TLRs and permeabilization of the phagolysosomal membrane allowing IgG and nuclear antigen to access the cytosol and activate innate sensors. Other enzymes that are critical in degrading nuclear antigens independent of lysosome function include RNase H2 (*149*), DNase I (*150, 151*), and variants of DNase III (TREX1) (*152*). These have been implicated in SLE and may operate in concert with impaired lysosomal maturation to promote autoimmunity. Collectively, these findings describe the underlying events promoting the accumulation of nuclear antigens and activation innate sensors that drive autoantibody, IFNα, and heightened apoptosis in SLE.

This study focused on defining how nuclear antigens accumulate on MFs, but since nuclear antigen accumulates on DCs, B, and T cells (*37*) it is possible that other cells might harbor defects in lysosomal maturation promoting other disease manifestations. For example, diminished lysosomal maturation in pDCs could heighten secretion of IFNα (*134*). In contrast, diminished lysosomal maturation in macrophages and neutrophils may heighten cell death (*153*). Further, the presence of nuclear self-antigens on the cell surface could impact B cell tolerance. For example, accumulation of nuclear antigens on the cell surface could provide a source of high avidity antigen that renews BCR signaling and activates autoreactive B cells (*154*), facilitates uptake of TLR ligands by BCR-mediated endocytosis (*89*), and positions autoreactive B cells to further differentiate into memory cells if T-help is available (*155*). Thus, the same overarching lysosomal defect may contribute to the activation of multiple cell types in SLE.

Overlapping autoimmune diseases are common in patients diagnosed with SLE including diabetes (*156*), rheumatoid arthritis (*157*), and Sjögren's syndrome (*158*). Recent GWAS studies have identified common genetic polymorphisms including the major histocompatibility complex, TNFAIP3, PTPN22 (*159*), STAT4 (*160*), and CD40 (*161*) that span multiple autoimmune diseases, although their functional role in breaking tolerance is unknown. Our finding that punctate IgG accumulates on MFs from multiple murine models of autoimmunity including SLE, diabetes, and rheumatoid arthritis is interesting as it might reflect a defect common to multiple autoimmune diseases. Further, the IgG did not colocalize with high levels of nuclear antigens, suggesting that the antigens contained in the IgG-ICs might be disease-specific, and as a result, activate the immune system in different ways. Therefore the accumulation of punctate IgG on the surface of MFs from NOD and K/BxN mice raises the possibility that impaired lysosomal maturation underlies other autoimmune diseases.

Materials and Methods

Mice

C57BL/6 (B6) and MRL/MpJ-*Tnfrs6*^{lpr}/J (MRL/*lpr*; JAX mice Stock # 000485) colonies were maintained in an accredited animal facility at University of North Carolina at Chapel Hill (UNC-CH). NZM2410 mice (*162*) were obtained from Dr. Gary Gilkeson, AID$^{-/-}$MRL/*lpr* mice (*163*) from Dr. Marilyn Diaz, NOD mice from Roland Tisch, and K/BxN mice (*164*) from Christophe Benoist, and C57BL/6-Tg(UBC-GFP)30Scha/J (GFP-expressing) mice (*165*) from Bill Goldman. We generated FcγRI$^{-/-}$MRL/*lpr* mice by backcrossing FcγRI$^{-/-}$C57BL/6 mice to MRL/*lpr* mice for 10 generations.

Reagents

Antibodies specific for LAMP1 and CD11b were purchased from BD Biosciences, LC3A from Cell Signaling, goat anti-rabbit IgG and rabbit anti-goat IgG from Molecular Probes; AIM2, ASC, TRIM21, p65, IRAK1, IRF3, and IRF7 from Santa Cruz Biotechnologies, anti-IgG from Jackson ImmunoResearch, and anti- LPS (E. coli J5) from Thermo Scientific. Concanamycin A and chloroquine diphosphate salt were purchased from Sigma-Aldrich, Immunogold conjugate EM streptavidin from BB International, and TNP_{20}KLH from Biosearch Technologies. Antibodies specific to Smith (Sm; 2.12.3), nucleosome (PL2-3) CD16/32 (2.4G2), and TNP (Hy1.2) were purified from hybridoma culture supernatant using protein G-Sepharose (GE Healthcare) then left unlabeled or conjugated with Alexa fluor according to the manufacturer instructions (Molecular Probes). Fluorescent molecules LysoSensor, dihydrorhodamine 123, and CellMask were purchased from Molecular Probes and FAM-FLICA caspase-1 assay kit from ImmunoChemistry Technologies. LI-COR blocking buffer and

IRDye680- and IRDy800-conjugated antibodies (anti-rabbit, anti-mouse, anti-goat) were purchased from LI-COR Biosciences.

Bone Marrow-derived MF (BMMF) cultures

Single-cell suspensions of bone marrow were prepared from the tibias and femurs of C57BL/6 mice. Mononuclear cells were isolated using Lympholyte Separation Medium (CEDARLANE Laboratories, Burlington, ON) plated in 60 mm petri dish with 6 mL macrophage differentiation media (DMEM with 10% FBS, 10% L-cell supernatant, 1 mM Sodium pyruvate, 50 μg/mL Gentamicin, 100 μg/mL Pen/Strep, 2mM L-Glutamine, 50 nM β-ME and cultured overnight (37°C, 5% CO_2). After the overnight culture, non-adherent cells were plated into non-tissue culture treated 100 mm petri dishes (0.75-1 mL cells/petri dish) and 7 mL fresh macrophage differentiation media was added to each dish. To promote macrophage differentiation, cells were incubated for 6 days (37°C, 5% CO_2). On day 4, culture medium was replenished with an additional 5 mL of macrophage differentiation media. The resulting bone marrow derived macrophages were removed from the dish by washing with ice cold PBS. BMMF cultures were 98% $CD11b^{+}$, I-A^{lo}, and B7.2^{lo}.

Formation of Immune Complexes

Apoptotic debris-containing immune complexes (IgG-IC): Single-cell suspensions of thymocytes were prepared from 5-8 week mice, irradiated (600 rads) and cultured 16-18 hours 10 mL PBS (37°C, 5% CO_2). Apoptotic thymocytes were centrifuged for 5 minutes (350 x g) and the supernatant containing apoptotic debris was incubated with autoantibodies (2.12.3 or PL2-3) on ice for 30 min (6.67 μg Ab/1 mL supernatant). Immune complexes were pelleted (160,000 x g) at 4°C for 45 min. Pelleted ICs were resuspended in 250 μL R10 media (RPMI

with 10% FBS, 1 mM Sodium pyruvate, 50 μg/mL Gentamicin, 100 μg/mL Pen/Strep, 2mM L-Glutamine, 50 nM β-ME).

TNP-containing immune complexes (TNP-ICs): To form TNP-ICs we incubated TNP_{20}-KLH with anti-TNP antibody (Hy1.2) on ice for 30 min (30 μg Ab/1 μg TNP-KLH). Immune complexes were pelleted (160,000 x g) at 4°C for 45 min then resuspended in 200 μL R10 media (as above).

Escherichia coli-containing immune complexes (*E. coli*-ICs): To form *E. coli-ICs* we incubated GFP-expressing *E. coli* (*166*) with anti-LPS at room temperature for 2 hours (1.5 μg/$6.25x10^6$ *E. coli*) in the presence of gentamycin (10 μg/1 mL). *E. coli*-ICs were cultured with BMMFs at a MOI of 25.

Fluorescent Microscopy

All confocal microscopy was conducted using a Zeiss 710 confocal microscope with a 63 × 1.4 NA (oil) PLAN APO lens and Zeiss Zen software. All 2-photon microscopy was conducted using an Olympus FlouView FV1000MPE multiphoton microscope with a 25 × 1.05 NA (water) XLPlan N lens and Olympus FluoView software. Data was analyzed using ImageJ.

IgG-IC/apoptotic bleb localization: BMMFs were cultured in the presence of apoptotic debris-containing IgG-Alexa488 ICs or GFP-expressing apoptotic debris for 2 hours in R10 media (as above). After 2 hours the media was aspirated and cells were cultured in fresh R10 media. CellMask and Hoechst 33342 were introduced to BMMFs 15 minutes prior to fixation at indicated time points. Cells were fixed in room temperature with 2% paraformaldehyde and transferred to 4°C for 15 min. Cells were resuspended in FluorSave and loaded onto coverslips for imaging. The membrane localization of IgG-ICs or apoptotic debris was quantified by

calculating the Mander's coefficient of colocalization (ratio of colocalized pixels/total fluorescent pixels).

2-photon microscopy/pH quantification: Two hours prior to imaging, BMMFs were incubated (37°C, 5% CO_2) on a glass bottom petri dish (MatTek Corp) in R10 media (rhodamine free RPMI with 10% FBS and pen/strep [as above]). Immediately after adding 40 μL of IgG-ICs and LysoSensor (2 mg/mL) cells were imaged for 1 hour. The dye was excited using two-photon excitation (710 nm) and emissions at 420-460 nm and 495-540 nm were quantitated. The ratio of the emission channels were used to determine the pH of the vesicles using a standard curve generated by exciting LysoSensor with medium of varying pH, then quantifying the ratio of the emission channels.

ASC localization/caspase-1 activation: BMMF were cultured with FAM-FLICA caspase-1 for 20 minutes, fixed with 2% paraformaldehyde at the indicated time points, then incubated at 4°C for 15 min. Cells were blocked in 2.4G2 for 30 min at 4°C, stained with an anti-ASC antibody and Hoechst 33342 (1 μg/ml) in permeabilization buffer (PBS with 0.05% Saponin and 0.5% BSA) for 30 min at 4°C. Cells were washed again, stained with goat anti-rabbit IgG-Alexa 647 in permeabilization buffer for 30 min at 4°C, washed, co-stained with anti-CD11b in FACS media (2% FBS, 0.02% NaN_3) for 30 min at 4°C, washed, resuspended in FluorSave and loaded onto coverslips for microscopic imaging. The number of cells with cytosolic ASC foci were counted and expressed as a percentage of the total cells. Total caspase-1 activation per cell was quantified, background fluorescence subtracted, and fluorescence was normalized by cell area.

LAMP1/LC3A, IRF, and p65 localization: BMMFs, or splenic myeloid cells ($CD11b^+$) purified by positive selection were prepared as described for ASC localization/caspase-1 activation except cells were stained for LAMP1 and LC3A, IRF3, IRF7, or p65. The nuclear

localization of IRF or p65 was quantified by calculating the Mander's coefficient of colocalization (ratio of colocalized pixels/total fluorescent pixels).

Flow Cytometry

All flow cytometry was conducted using an 18-color Becton Dickinson LSR II Flow cytometer and data were acquired using Becton Dickinson FACSDiva 8.0.1 software.

Recycling flow: BMMFs were incubated (37°C, 5% CO_2) with 40 μL Alexa488-labeled IgG-ICs in R10 media (as above). To quantify surface bound ICs at 0 hours, phagocytic uptake was impaired by culturing with IgG-ICs on ice for 2 hours. This was sufficient to allow the ICs to bind to the surface of the cell but not be phagocytosed. For all other time points, cells were incubated (37°C, 5% CO_2) for 2 hours, then media was replaced to remove all unbound ICs. At indicated time points, cells were blocked in 2.4G2 for 30 min on ice, washed and split into 2 samples. One sample was incubated with an anti-Alexa488 antibody (quenches Alexa488 fluorescence), while the other sample was left in FACS media (as above) for 30 min on ice. Both samples were washed and fixed with 2% paraformaldehyde, and then incubated at 4°C for 15 min. Cells were resuspended in FACS media and the levels of surface IgG-IC were quantified by flow cytometry. External IgG-ICs were calculated by subtracting the Alexa488 quenched sample (internal IgG-ICs) from the unquenched sample (total IgG-ICs).

Ratiometric flow cytometry: BMMFs were incubated (37°C, 5% CO_2) for 2 hours prior to the addition of 40 μL of IgG-ICs in R10 media (as above). Concanamycin A (20 ng/mL) was introduced to one sample from each cell type as a way to quantify an unacidified cell 2 hours prior to addition of IgG-ICs and left on the cells throughout the experiment. IgG-ICs and LysoSensor (2 mg/mL) were introduced for 30 min, aspirated, and replaced with fresh rhodamine free R10 media. Cells were incubated until indicated time points and analyzed by

flow cytometry. A UV laser (355 nm) was used to excite the dye and the MFI from the emission channels (450/20 nm, 585/42 nm) was ratioed to quantify relative pH.

Ex vivo surface stain: *Ex-vivo* Splenic cells were fixed in room temperature 2% paraformaldehyde and incubated for 15 minutes at 4°C. Cells were blocked in 2.4G2 for 30 min at 4°C, washed, stained with anti-Sm (2.12.3) in FACS media (as above) for 30 min at 4°C, washed, stained with anti-CD11b in FACS media for 30 min at 4°C, and washed. Cells were resuspended in FACS media and the MFI of the surface Sm was determined by flow cytometry and normalized to an isotype control.

Ex vivo caspase-1 activation: *Ex-vivo* splenic cells incubated with FAM-FLICA caspase-1 (5 μM) 20 minutes prior to fixation in FACs media (as above) at room temperature. Cells were fixed in room temperature with 2% paraformaldehyde and transferred to 4°C for 15 min. Cells were then blocked in 2.4G2 for 30 min at 4°C, washed, stained with anti-CD11b in FACS media for 30 min at 4°C, and washed. Cells were resuspended in FACS media and caspase-1 activation was determined by quantifying the MFI by flow cytometry.

Cryo-Electron Microscopy

BMMFs were incubated with 40 μL of gold-labeled IgG-ICs for 2 hours (37°C, 5% CO_2). Suspensions of macrophages were loaded into gold planchettes (model 16706897, well size 1.2 mm x 200 μm), which were placed in high-pressure-freeze (HPF) holders and torqued to make a tight seal. Each sample was placed in the HPF chamber where the pressure was increased with cyclohexane to about 2000 bar just milliseconds before a blast of liquid nitrogen cooled the assembly at about 18,000 degrees/sec using a Leica EM PACT HPF. The pressure and cooling curves were recorded and examined after each run to ensure consistency. Frozen samples were transferred to liquid nitrogen for storage. The samples were then transferred to vials containing

2% osmium tetroxide in dry acetone cooled in liquid nitrogen. The vials were transferred cold to a chamber at -90 °C in a Leica EM AFS freeze substitution device, where samples remained for 72 hours. The samples were warmed automatically using a program that increased the temperature to -20 °C at 4 degrees/hour, held at -20 °C for 10 hours, then warmed at 4°/hour to 20°C. The warmed fixed samples were processed for transmission electron microscopy (TEM) by washing with fresh acetone and replacing the acetone with propylene oxide, then embedding in epon (EMS EMbed-812) and hardening at 60 °C. Thin sections, about 60-70 nm thick, were cut with a diamond knife on a Leica Ultracut UTC and stained with uranyl acetate and lead citrate. Stained thin sections were examined with an FEI Tecnai T12 G2 TEM at 80 kV using a Gatan 794 digital camera and Gatan Digital Montage software to prepare up to 5x5 montages of selected macrophages imaged at 6,000x to 30,000x.

Immunoprecipitation and Western Blot

Lysates were prepared by the addition of lysis buffer containing 1% CHAPS, 150 mM NaCl, 10 mM Tris (pH 7.5), 2 mM sodium orthovanadate, 1 mM PMSF, 0.4 mM EDTA, 10 mM NaF, and 1 μg/ml each of aprotinin, leupeptin, and α1-antitrypsin to cell pellets. Lysates were held on ice for 10 min followed by the removal of particulate material by centrifugation at 12,000 × *g* for 10 min at 4°C.

Antibodies used in the immunoprecipitations were conjugated to cyanogen bromide-activated Sepharose 4B according to manufacturer's instruction (Amersham Pharmacia Biotech). Approximately 2 μg of precipitating antibodies was incubated with 1.5×10^6 cell equivalents of cleared lysate for 1 hour at 4°C. Immunoprecipitates were washed twice with lysis buffer, resuspended in reducing SDS-PAGE sample buffer, and then fractionated by 10% SDS-PAGE. Separated proteins were transferred to Immobilon-FL membranes. Membranes were blocked in

Li-cor Blocking Buffer, then incubated with the various immunoblotting Abs followed by the appropriate fluorophore-conjugated secondary Abs. Immunoreactive proteins were detected using a LI-COR Odyssey infrared imaging system with Odyssey 3.0 software.

Plate Reader

All analysis was conducted using a Tecan M200 fluorescence plate reader.

ROS Assay: BMMFs were incubated (37°C, 5% CO_2) for 2 hours prior to the addition of 40 μL of IgG-ICs in R10 media (as above) in an opaque 96 well plate. 30 minutes prior to indicated time points, dihydrorhodamine 123 (3 μg/mL) was added to each well. At the indicated time points cells were washed and fixed in room temperature with 2% paraformaldehyde and transferred to 4°C for 15 min. Wells were analyzed in FACS media (as above). All fluorescent readings were normalized to the background fluorescence of non-DHR treated cells.

Immunoprecipitation Assay: All beads from immunoprecipitation sample were added to a single well in a an opaque 96 well plate in PBS. Wells were analyzed for Hoechst labeled dsDNA (AIM2 immunoprecipitation) and Alexa647 labeled IgG (TRIM21 immunoprecipitation). All fluorescent readings were normalized to the background fluorescence of beads alone.

WISH cell IFNα assay

WISH cells, a human epithelial cell line (product no. CCL-25; American Type Culture Collection, Manassas, VA), were grown in minimum essential medium supplemented with L-glutamine (2 mM), HEPES (20 mM*),* penicillin (100 units/ml), streptomycin (100 ug/ml), and 10% fetal bovine serum (37°C, 5% CO_2). To measure the levels of IFNα in the serum, we quantitated mRNA of interferon regulated genes as previously described (*167*). WISH cells were plated at a density of 0.5 x 10^5/0.1 ml in 96-well flat bottom plates and cultured with media alone, recombinant mouse IFNα (BioSource International, Camarillo, CA) at 100 units/ml, or

BMMF supernatant (200 µL). After 24 hours of incubation, WISH cells were lysed, RNA extracted (RNeasy Mini Kit; Qiagen, San Diego, CA) and cDNA prepared from 500 ng of RNA (iScript c-DNA Synthesis Kit; Bio-Rad Laboratories, Hercules, CA). The cDNA obtained from each sample was diluted 1:60, and 2 µl was amplified in a 20 µl real-time quantitative PCR reaction using 10 mM forward and reverse primers and the 2x iQ SYBR Green Supermix (Roche laboratories).

Figures

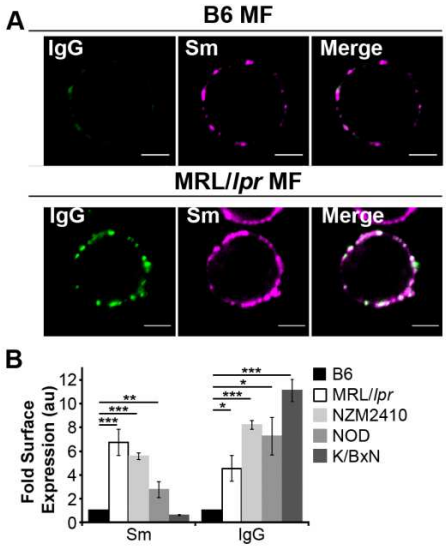

Figure 1. Autoimmune-prone MFs have accumulated IgG-ICs on the cell membrane.

Splenic CD11b+ cells were harvested from the indicated mice and analyzed for surface Sm and IgG by confocal imaging (Bar=2.5 μm); data represent 5 experiments, 5-7 mice, 55-75 cells (**A**) and flow cytometry; 4 experiments, 4-7 mice (B6≥12 wks, MRL/*lpr*≥12 wks, NZM2410≥12 wks, NOD≥26 wks, K/BxN≥13 wks) (**B**). Error bars indicate standard error of the mean (SEM). Student *t* test, **p*≤0.05, ***p*≤0.01, ****p*≤0.001.

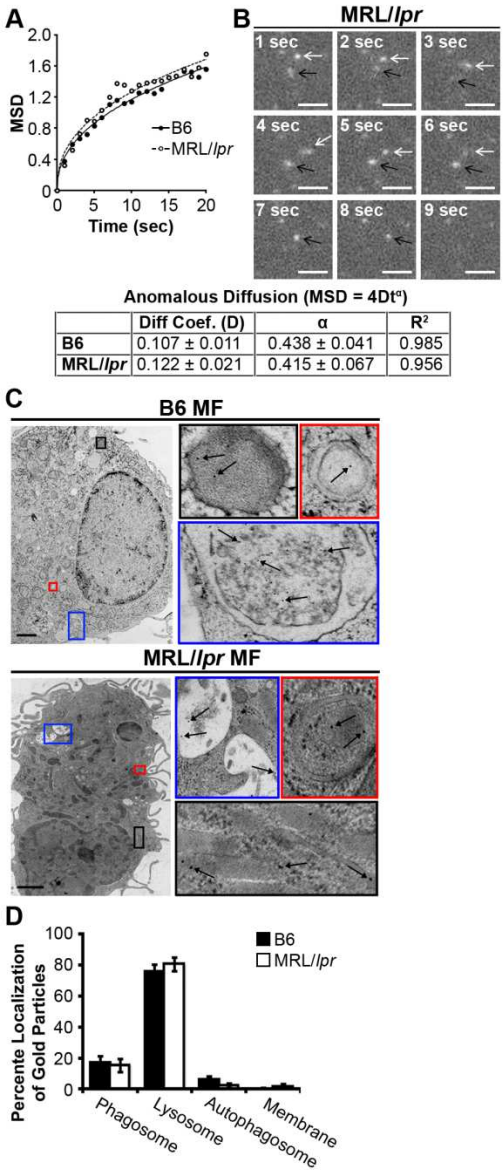

Figure 2. MRL/*lpr* MFs phagocytose and traffic IgG-ICs to lysosomal structures. BMMFs from the indicated mice were cultured with fluorescently-labeled IgG-ICs and examined over time by total internal reflection fluorescence (TIRF) microscopy (Bar=1 μm); 3 experiments, 3 mice, n=60-81 (**A-B**). The mean squared displacement (MSD) was calculated by tracking the displacement of IgG-ICs (arrows) on the surface of the cell until the IgG-IC was phagocytosed and left the plane of imaging. Each point is the average MSD of 10-20 IgG-ICs from 2-5 cells in the imaging plane (**A**). BMMFs from the indicated mice were cultured with gold-labeled IgG-ICs for 2 hours and examined by cryo-electron microscopy (Bar=1 μm); 2 experiments, 2 mice,12-15 cells (**C-D**). IgG-ICs were found in phagosomes (single membrane, electron light), lysosomes (single membrane, electron dense), autophagosomes (double membrane), and on the cell membrane. Error bars=SEM. Student *t* test, **p*≤0.05, ***p*≤0.01, ****p*≤0.001.

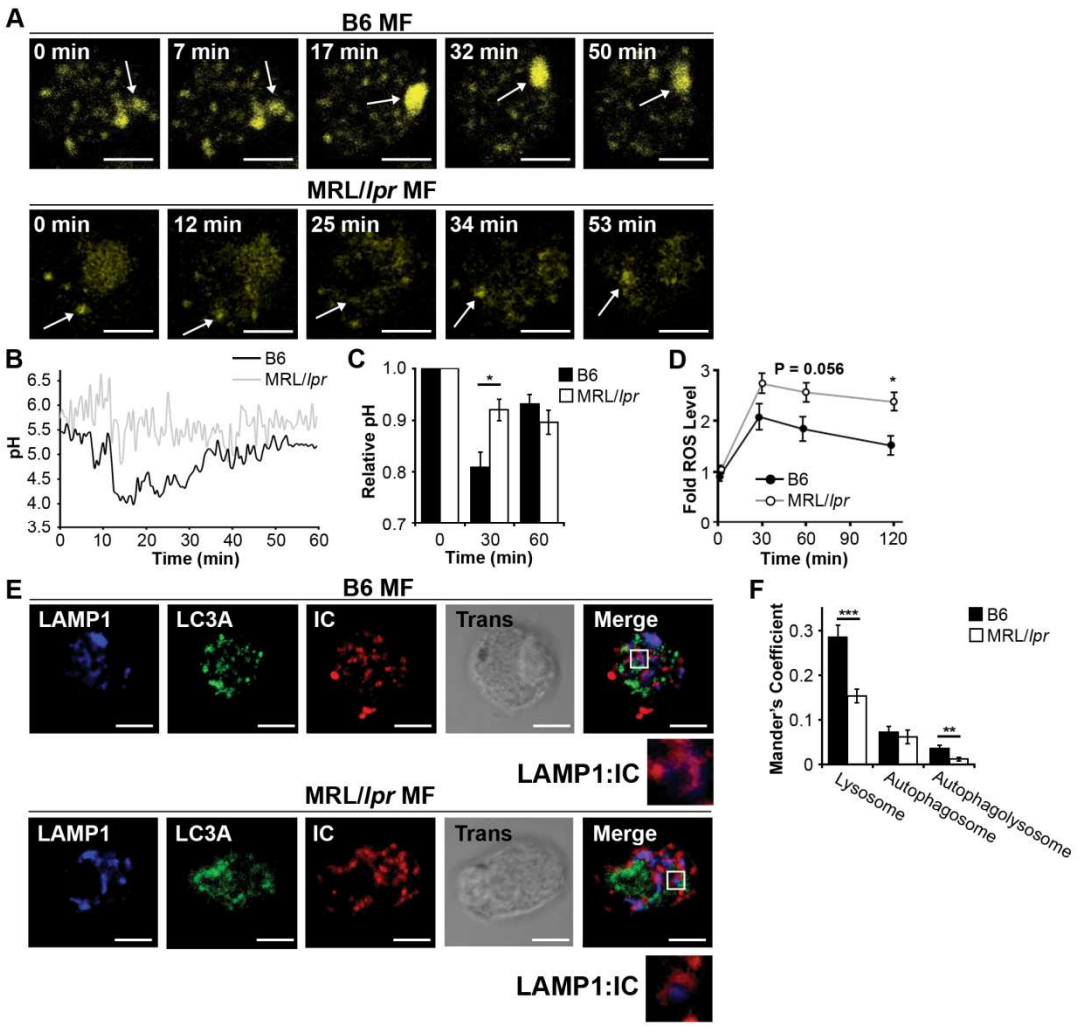

Figure 3. MRL/*lpr* MFs fail to mature the lysosome. Bone marrow derived macrophages (BMMFs) stimulated with IgG-ICs and vesicles (arrow) were assessed for lysosomal pH by real time ratiometric 2-photon microscopy (Bar=5 μm); 3 experiments, 3 mice, 25-40 cells (**A**-**B**), and ratiometric flow cytometry; 6 experiments, 6-8 mice (**C**), intracellular ROS levels were quantified over time by fluorescence plate reader; 6 experiments, 6 mice and (**D**), and co-localization of IgG-ICs with LAMP-1 and/or LC3A by confocal imaging (Bar=5 μm); 3 experiments, 3 mice, 36-39 cells (**E**-**F**). Error bars indicate standard error of the mean (SEM). Student *t* test, *$p \leq 0.05$, **$p \leq 0.01$, ***$p \leq 0.001$.

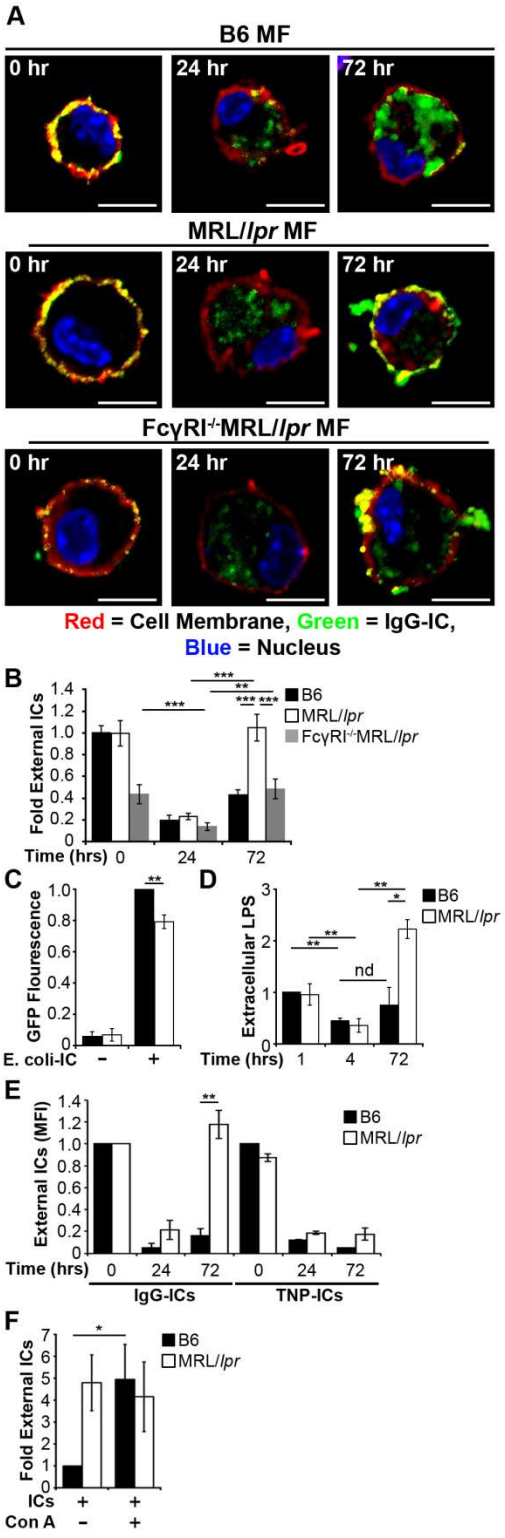

Figure 4. IgG-ICs recycle and accumulate on the cell membrane of MRL/*lpr* MFs. BMMFs from the indicated mice were cultured with IgG-ICs and examined over time by confocal imaging (Bar=5 μm); 4 experiments, 3-4 mice, 17-23 cells (**A**-**B**). BMMFs stimulated (1 hour) with dead GFP-expressing *E. coli* opsonized by IgG (*E. coli*-ICs) were analyzed by flow cytometry for relative amounts of phagocytosed *E. coli*-ICs (**C**) and at indicated time points for extracellular LPS; 3 experiments, 3 mice (**D**). Flow cytometry localizing fluorescent IgG-ICs and TNP-ICs over time; left panel: 5 experiments, 5 mice; right panel: 2 experiments 2 mice (**E**). BMMFs cultured in the presence or absence of concanamycin A (20 ng/ml) were exposed to fluorescently-tagged IgG-ICs for 72 hours and then assessed for surface fluorescence by flow cytometry; 5-6 experiments, 5-6 mice (**F**). Error bars=SEM. Student *t* test, *$p \leq 0.05$, **$p \leq 0.01$, ***$p \leq 0.001$.

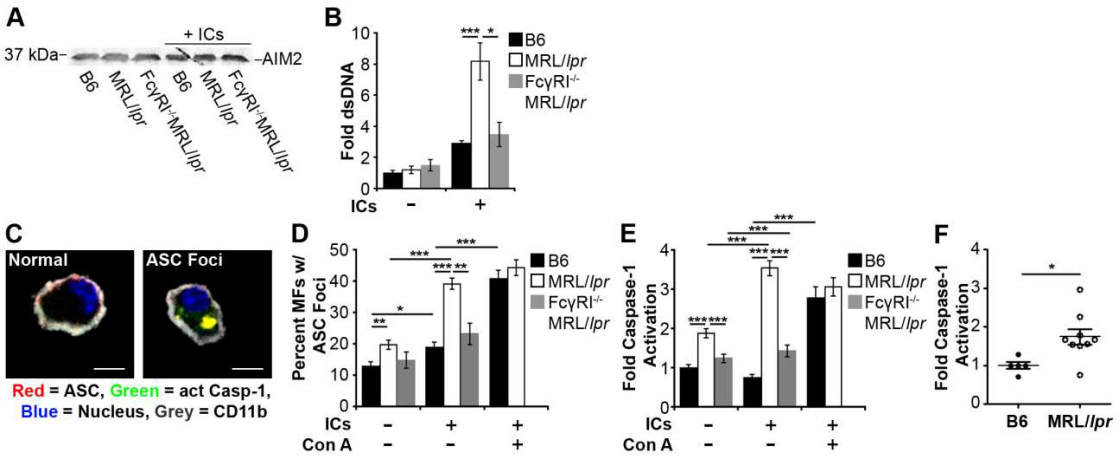

Figure 5. Impaired lysosomal maturation allows dsDNA to leak into the cytosol and activate AIM2. BMMFs were stimulated for 4 hours with Hoechst-labeled IgG-ICs (**A-B**). Following AIM2 immunoprecipitation (5-8x10^6 cells), fluorescent DNA was quantified and expressed as fold increase relative to unstimulated B6. A representative AIM2 immunoblot of immunoprecipitated protein (**A**); Data are representative of 4 experiments, 4 mice. BMMFs were stimulated for 4 hours with IgG-ICs in the presence or absence of concanamycin A (20 ng/mL). Cells were examined by confocal imaging for the formation of ASC foci (Bar=5 μm); 10 experiments; 2-10 mice, 63-364 cells (**C-D**), and the activation of caspase-1; 10 experiments; 2-10 mice, 63-257 cells (**E**). Data are normalized to caspase-1 activation in unstimulated B6 MFs. Caspase-1 activation was measured in B6 and MRL/*lpr* splenic myeloid cells ($CD11b^+$) by flow cytometry; 4 experiments, 5-9 mice (≥17 wks; active disease confirmed with kidney H&E) (**F**). Error bars=SEM. Student *t* test, *$p \leq 0.05$, **$p \leq 0.01$, ***$p \leq 0.001$.

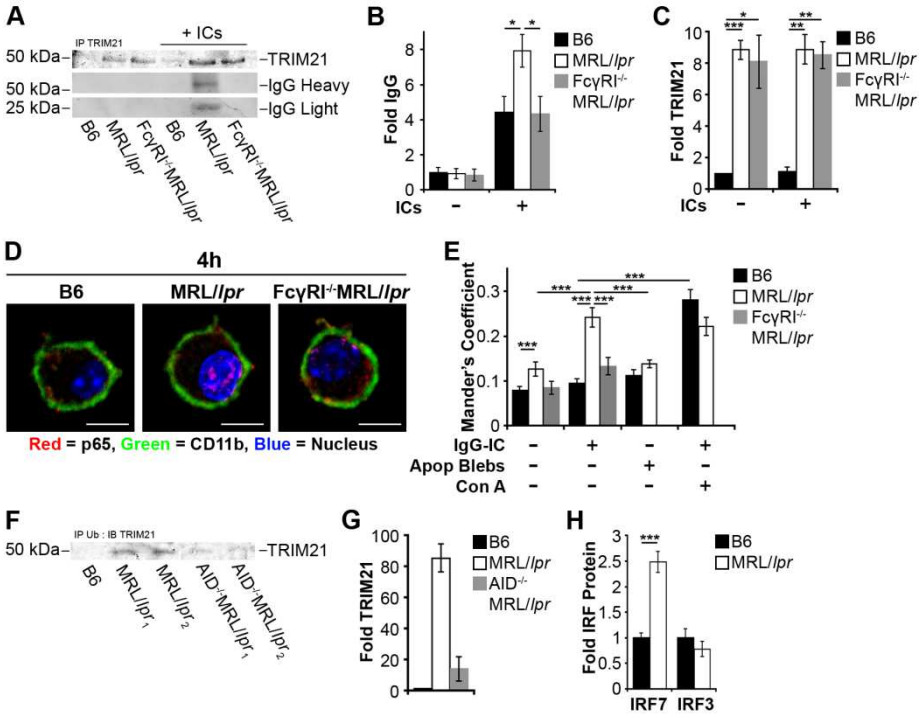

Figure 6. Impaired lysosomal maturation allows IgG to leak into the cytosol and activate TRIM21. BMMFs were stimulated for 4 hours with IgG-ICs containing fluorescently tagged IgG. Following TRIM21 immunoprecipitation (5-8x10^6 cells), fluorescent IgG was quantitated and expressed as fold increase relative to unstimulated B6; 7 experiments, 7 mice (**A-B**) and IgH/IgL and immunoprecipitated TRIM21 protein levels were immunoblotted (**A**) and quantitated by densitometry; 3 experiments, 3 mice (**A,C**). Nuclear translocation of the p65 subunit of NF-κB was quantified in BMMFs stimulated for 4 hours with IgG-ICs or apoptotic debris (lacking IgG) untreated or treated with concanamycin A (20 ng/mL) (Bar=5 μm); 6 experiments, 3-6 mice, 16-57 cells (**D-E**). Ubiquitin was immunoprecipitated from splenic myeloid cells ($CD11b^+$; 35x10^6 cells) and the levels of ubiquitinated TRIM21 were assessed by immunoblot; 2 experiment, 4-5 mice (≥17 wks; active disease confirmed with kidney H&E) (**F-G**). Splenic myeloid cells ($CD11b^+$) were analyzed for IRF7 and IRF3 protein by confocal microscopy; 2 experiments, 2 mice, 10-28 cells (**H**). Error bars=SEM. Student *t* test, *$p \leq 0.05$, **$p \leq 0.01$, ***$p \leq 0.001$.

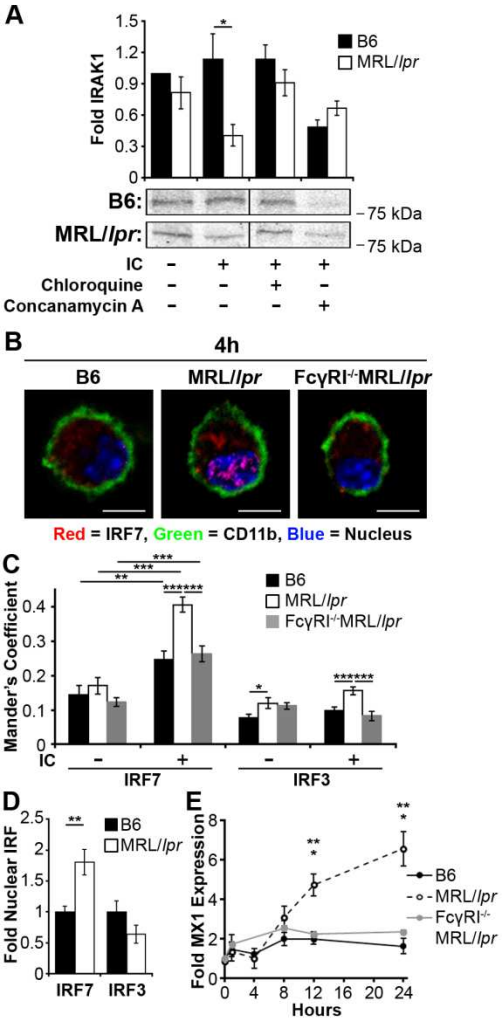

Figure 7. Impaired lysosomal maturation promotes intracellular TLR activation and IFNα secretion. BMMFs (1-1.5x10^6 cells) from B6 and MRL/*lpr* mice were stimulated for 24 hours with IgG-ICs in the presence or absence of hydroxychloroquine (50 μg/mL) or concanamycin A (20 ng/mL). IRAK1 levels were quantitated from cell lysates by immunoblot, a representative IRAK blot is shown with densitometry quantitation from 5 experiments, 3-5 mice (**A**). BMMFs from the indicated mice were stimulated with IgG-ICs for 4 hours. Nuclear translocation of IRF7 and IRF3 were quantified by confocal microscopy (Bar=5 μm); 4 experiments, 3-4 mice, 20-42 cells (**B-C**). Nuclear IRF7 and IRF3 were quantified in *ex vivo* splenic myeloid cells ($CD11b^+$) by confocal imaging. Data are displayed as fold increase relative to unstimulated B6; 2 experiments, 2 mice (≥17 wks; active disease confirmed with kidney H&E), 10-28 cells (**D**). BMMFs from the indicated mice were stimulated with IgG-ICs. Supernatants were collected at the various time points and cocultured with WISH cells for 24 hours. MX1 message levels were quantified by RT-PCR and displayed as fold increase relative to unstimulated B6. Error bars=SEM. Student *t* test, *$p \leq 0.05$, **$p \leq 0.01$, ***$p \leq 0.001$.

Supplemental Figures

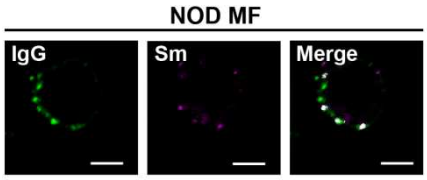

Fig. S1. IgG and Sm staining is punctate on the surface of NOD myeloid cells. Splenic myeloid cells ($CD11b^+$) were purified from NOD mice and analyzed for surface levels of Sm and IgG by confocal microscopy (Bar=5 μm); 2 experiments, 2 mice, 15-20 cells.

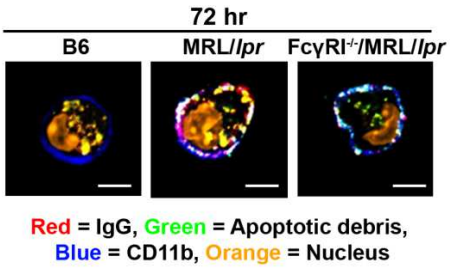

Fig. S2. IgG and apoptotic debris remain colocalized upon recycling of IgG-ICs. BMMFs from the indicated mice were cultured with fluorescently-labeled IgG-ICs and examined over time by confocal microscopy (Bar=5 μm); 2 experiments, 2 mice,15-20 cells. IgG-ICs were formed using Alexa 647-labeled IgG and GFP-expressing apoptotic thymocytes.

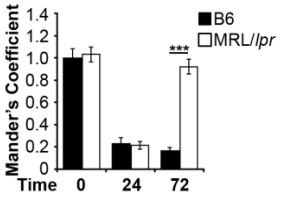

Fig. S3. MRL/*lpr* MFs recycle apoptotic blebs. BMMFs from the indicated mice were cultured with apoptotic blebs (no IgG) and examined over time by confocal imaging; 3 experiments, 3 mice, 19-31 cells. Apoptotic blebs were formed from GFP-expressing thymocytes.

CHAPTER 3: Chronic mTOR activation impairs lysosome maturation in lupus-prone macrophages

Lysosomes contribute to immunological homeostasis by degrading biomolecules including apoptotic debris internalized by phagocytosis. In a model of systemic lupus erythematosus (SLE) where diminished lysosomal maturation promotes the accumulation of surface IgG-immune complexes, we find that mTOR plays a key role in lysosomal maturation by activating caspase-1 through an actin-dependent mechanism. Cofilin acts as a key regulator in this process as its phosphorylation controls the levels of caspase-1 activation and hence the cleavage of Rab39a, a necessary step for lysosomal maturation. These data identify a previously undescribed signaling pathway regulating lysosomal maturation and revealing potential therapeutic targets in restoring the clearance of apoptotic debris in SLE.

Introduction

Lysosomes contain proteases and lipases that play a critical role in cell homeostasis and metabolism by degrading macromolecules. Degradation requires that intracellular and extracellular cargo traffic to the late endosomes, that late endosomes fuse with lysosomes promoting maturation, and that the hydrolases become activated through lysosomal acidification; a processes that requires Rab proteins, ESCRT complexes, ubiquitination, vacuolar H+-ATPase (V-ATPase), and LAMPs. The signal transduction events that control the lysosomal environment are unknown; however, lysosomal defects are associated with cardiovascular disease, lysosomal storage disorders, cancer, and neurodegenerative disorders (*168*). In addition, we recently reported that macrophages (MFs) from systemic lupus erythematosus (SLE)-prone

mice harbor a lysosomal maturation defect that diminishes lysososmal acidification. As a consequence, FcγRs bound by immune complexes (ICs) composed of apoptotic debris bound by IgG autoantibody (IgG-ICs) recycle and accumulate on the cell surface. They also leak into the cytosol heightening cell death, IFNα secretion (*169*), autoantibody production, and lupus nephritis (*37*). Herein we identify a novel signal transduction pathway that regulates lysosomal maturation, and underlies the reduced ability of lupus-prone MFs to degrade apoptotic debris.

Heightened and mislocalized mTOR activity impairs lysosomal maturation in lupus-prone MFs

IgG-ICs, formed between apoptotic debris and autoantibody, are thought to play a central role in SLE. We recently reported that macrophages from MRL/lpr mice fail to degrade IgG-ICs phagocytosed through FcgRs (*37*). To assess whether this leads to chronic FcgR-mediated signal transduction that might impair lysosomal maturation, we quantitated the levels of phosphorylated signaling effectors coupled to ITAM-containing FcgRs. Consistent with the findings in T cells (*170, 171*), bone marrow MFs (BMMFs) derived from lupus-prone MRL/*lpr* mice had 5-fold more pS6 compared to B6 (Fig 1A), indicating that MRL/*lpr* MFs have heightened mammalian target of rapamycin (mTOR) activity. Furthermore, MRL/*lpr* MFs have 2.8-fold more $pAkt^{S473}$ and 2.3-fold more $pAkt^{T308}$ compared to B6 (Fig 1A). The activation of Akt was dependent on FcγR-signaling because pAkt was not significantly elevated in $Fc\gamma RI^{-/-}$/MRL/*lpr* MFs; however the proportion of pS6 was reduced to 2-fold above B6 (Fig 1B) indicating that mTOR is in part activated by FcgRI, but a second pathway is also involved. The heightened mTOR activity is not driven by AMPK since phosphorylated and total AMPK were not significantly elevated in MRL/*lpr* MFs (Fig 1C). Interestingly the addition of IgG-ICs induced heightened mTOR

activation but did not induce heightened AKT activation above basal levels (Fig 1C) indicating that AKT is chronically active in MRL/*lpr* MFs.

The serine/threonine kinase mTOR senses amino acids and ATP to balance cell growth and nutrient availability (*172*). The subcellular localization of mTOR to The subcellular localization of mTOR is critical for its function. For example, localization of mTOR to the cell membrane is important for insulin signaling and cytoskeletal rearrangements, while localization to the membrane of lysosomal compartments is important in amino acid sensing (*173*). Therefore identifying the localization of mTOR in MRL/*lpr* MFs may elucidate its function. Strikingly, MFs from MRL/*lpr* mice localized 3.5-fold more mTOR to the cell membrane compared to B6 MFs (Fig 1C-D). This difference in localization was not the result of heightened total levels of mTOR (Fig 1E). Torin1 is a selective ATP-competitive inhibitor of mTOR that unlike rapamycin, inhibits both mTOR complex 1 (mTORC1) and mTORC2 (mTORC1/C2) (*174*) (Sup 2). Treatment of MRL/*lpr* MFs with Torin1 reduced the colocalization of mTOR with the plasma membrane to levels similar to B6 (Fig 1C-D). This indicates that activation of mTOR in MRL/lpr MFs, directly or indirectly promotes its chronic localization at the cell membrane.

We've previously identified that 80% of internalized IgG-ICs traffic to secondary lysosomes, with less than 5% entering autophagosomal structures (*169*). Since greater than 80% of internalized IgG-ICs traffic to secondary lysosomes and because mTOR localizes with lysosomal structures in sensing amino acid levels (*175*) it was possible that mTOR regulates the lysosomal environment. One possibility is that lysosomal maturation requires mTOR, and that a vicious cycle is created in lupus-prone MFs because of diminished degradation of IgG-ICs. The chronic, high level of ICs that remain bound to FcgRs chronically activates mTOR and its

mislocalization at the plasma membrane could perpetually impair lysosomal maturation. Since acidification of the phagolysosomal compartment is an integral step in lysosome maturation and the activation of lysosomal hydrolases (*73*), we previously determined the relative pH of the maturing phagosome using an acidotropic ratiometric dye during phagocytosis of IgG-ICs. Ratiometric flow cytometry 30 minutes after exposure to IgG-ICs, MRL/*lpr* MFs showed an 8% drop in pH compared to a 22% decline in B6 MFs indicating significantly impaired vesicular acidification (*169*), Fig 1F). Treatment of MRL/*lpr* MFs with Torin1 restored acidification to levels comparable to B6. Cells remained acidified for the duration of Torin1 treatment (Fig 1F). Further, Torin1 of MRL/*lpr* MFs prevented the recycling and accumulation of fluorescently labeled-IgG-ICs (Fig 1G). Interestingly, Torin1 treatment reduced the basal levels of IgG-ICs on B6 MFs suggesting that Torin1 enhances the degradative capacity of the lysosome (Fig 1G). Torin1 inhibits both mTORC1 and mTORC2 (*174*) while rapamycin inhibits only mTORC1 (*176*) (Fig S1). To determine which complex was impairing lysosomal acidification, we treated MRL/*lpr* MFs with rapamycin to determine whether it was sufficient in restoring acidification following internalization of IgG-IC. Rapamycin treated MRL/*lpr* MFs did not acidify (Fig 1F), suggesting that inhibition of mTORC1 is not sufficient in restoring lysosomal acidification. Given the strong effect of Torin1, this implicates mTORC2 in lysosomal acidification.

Heightened mTOR activity impairs lysosome maturation by driving the phosphorylation of cofilin

One important function of mTORC2 is to regulate actin by activating Rho GTPases (*176, 177*). Consistent with a role for the activation of mTORC2 in SLE, we found that MFs from MRL/*lpr* mice show impaired migration and membrane ruffling (Fig S2). Actin dynamics have been associated with the integrity of the lysosome (*178-180*) although how this occurs is unclear.

Despite this, it raises the possibility that chronic activation of mTORC2 might impair lysosomal acidification through an actin-dependent mechanism. mTORC2 activates Lim kinases (LIMKs) which in turn phosphorylate cofilin (Ser3). Prior to the addition of IgG-ICs, the proportion of p-cofilin in MRL/*lpr* MFs was 1.5-fold higher than B6 MFs (Fig 2A). After 30 minutes of stimulation with IgG-ICs, the proportion of p-cofilin increased 2.4-fold in MRL/*lpr* MFs. Treatment with the LIMK inhibitor (LIMKi 3) reduced the proportion of p-cofilin in MRL/*lpr* MFs to levels comparable to B6. Consistent with the idea that mTOR is upstream of LIMk, treatment with Torin1 also reduced p-cofilin in MRL/lpr MFs to levels comparable to B6, while treatment with rapamycin had no effect. Therefore, chronic activation of mTORC2 promotes heightened phosphorylation of cofilin in MRL/*lpr* MFs.

Cofilin depolymerizes F-actin by attaching to the minus-end, severing the actin filament, while phosphorylation of cofilin prevents its association with F-actin (*181, 182*). In MRL/*lpr* MFs, the heightened mTOR activity at the membrane (Fig 1C-D) increased the proportion of p-cofilin (Fig 2A). This would prevent the association of cofilin with the phagocytic cup and vesicles containing IgG-ICs. Following phagocytosis of IgG-ICs, B6 MFs localized 3.9-fold more cofilin to IgG-IC-containing vesicles compared to MRL/*lpr* (Fig 2B-C). In B6 MFs the cofilin that localized to IgG-IC-containing vesicles was rarely phosphorylated. Conversely, MRL/*lpr* MFs had 2.7-fold more p-cofilin colocalizing with vesicles containing IgG-IC. This indicates that the reduced levels of cofilin that localized to vesicles containing IgG-ICs were phosphorylated, and hence ineffective at depolymerizing actin.

If the depolymerization of F-actin were important in the maturation of the lysosome, we would expect that decreasing actin depolymerization by cofilin would restore acidification in MRL/lpr MFs. Conversely, it would inhibit acidification in B6 MFs. Jasplakinolide (JasP) binds

directly to F-actin and stabilizes actin filaments preventing depolymerization by cofilin. B6 MFs treated with JasP showed diminished lysosomal acidification only achieving a pH comparable to that found in MRL/*lpr* MFs (pH ~ 5.5). In contrast, inhibiting LIMK (LIMKi 3) increases cofilin-mediated depolymerization of F-actin. MRL/*lpr* MFs treated with LIMKi 3 restored acidification in MRL/*lpr* MFs, achieving pH levels comparable to B6 MFs (pH ~ 4) (Fig 2D). These data show that the depolymerization of F-actin by cofilin is integral to lysosomal acidification, and that this mechanism is defective in SLE.

Phosphorylation of cofilin prevents the recruitment of caspase-11 to vesicles containing IgG-ICs

Caspases have been strongly associated with driving cell death but recently caspases have been found to have alternative roles in the cell (*183*). Caspase-11 associates with F-actin through Aip-1 and cofilin to facilitate actin depolymerization (*184*). Since cofilin exhibits heightened phosphorylation and is mislocalized in MRL/*lpr* MFs (Fig 2A-C), the subcellular distribution of caspase-11 might also be altered. We found that phagocytosis of IgG-ICs induced B6 MFs to localized 3-fold more caspase-11 with vesicles containing IgG-IC compared to MRL/*lpr* (Fig 3A-B). This was not the result of heightened total caspase-11 (Fig 3C). Torin1 treatment was sufficient in restoring normal caspase-11 localization with vesicles containing IgG-ICs in MRL/*lpr* MFs, while rapamycin had no effect. This implicates activation of mTORC2 in the phosphorylation of cofilin and the mislocalization of caspase-11.

Since there is a heightened concentration of F-actin in the phagocytic cup, the recruitment of caspase-11 to the maturing phagosome may be integral in downstream acidification. It has been demonstrated that caspase-1 and caspase-11 are important in promoting acidification of the lysosome following phagocytosis of certain bacteria (*185, 186*) but the underlying mechanism

has not been characterized and whether caspase activity are necessary following the phagocytosis of IgG-ICs is unknown. We reasoned that if caspase-11 plays a role in lysosomal acidification following internalization of IgG-ICs, B6/*casp11*$^{-/-}$ MFs would show impaired acidification. Following phagocytosis of IgG-ICs, B6/*casp11*$^{-/-}$ MFs did not fully acidify, achieving a pH comparable to MRL/*lpr* MFs (Fig 3D). This demonstrates that caspase-11 is necessary for lysosomal acidification following the phagocytosis of IgG-ICs.

Recruitment of caspase-11 activates caspase-1

Caspase-11 physically interacts with, and activates, caspase-1 (*185, 187*). This implicates caspase-11 as an upstream regulator of caspase-1, and raises the possibility that the localization of caspase-11 with vesicles containing IgG-IC activates caspase-1 upstream of lysosomal acidification. To quantify caspase-1 activation, we stimulated MRL/*lpr* MFs with IgG-ICs in the presence of a FLICA probe specific to caspase-1. This allowed us to quantify caspase 1 activation by flow cytometry. We found that prior to the addition of IgG-ICs, MRL/*lpr* MFs show slightly elevated levels of basal caspase-1 activation compared to B6 MFs (Fig 3E). After phagocytosis of IgG-ICs, B6 MFs increased the levels of caspase-1 activation 2.1-fold. In contrast, MRL/*lpr* MFs did not change their levels of active caspase-1. The activation of caspase-1 in B6 MFs was dependent on caspase-11 because B6/*casp11*$^{-/-}$ MFs failed to activate caspase-1. Furthermore, MFs from B6/*pycard*$^{-/-}$ (ASC-deficient) mice activated caspase-1 to levels similar to B6 MFs. This indicates that during lysosomal acidification caspase-1 activation occurs independent of inflammasomes.

Following phagocytosis of IgG-ICs, we show that the localization of caspase-11 to IgG-IC-containing vesicles requires cofilin activity (Fig 3B). Further, caspase-11 is necessary for the activation of caspase-1 following phagocytosis of IgG-ICs (Fig 3E). To further assess whether

these events are linked, we altered the function of cofilin and assessed whether it impacted caspase-1 activation. We found that inhibiting the depolymerization of actin (JasP) in B6 MFs reduced the activation of caspase-1 to levels similar to MRL/*lpr* (Fig 3F). Conversely, inhibiting LIMK and the phosphorylation of cofilin allowed MRL/*lpr* MFs to activate caspase-1 to levels comparable to B6. These results demonstrate that activation of caspase-1 is dependent on actin depolymerization.

mTORC1 has multiple cellular functions including sensing amino acids and regulating translation (*172*), while mTORC2 is associated with AKT phosphorylation (S^{473}) and activating Rac1 and RhoA (*176, 177*). One possibility is that mTORC2 plays a previously unappreciated role in actin stabilization and lysosomal acidification. This predicts that inhibiting mTORC2 would restore activation of caspase-1 in MRL/*lpr* MFs. Indeed, treatment of MRL/*lpr* MFs with Torin1 promoted a 2-fold increase in caspase-1 activation following phagocytosis of IgG-ICs (Fig. 3G) while rapamycin had no effect. While this does not rule out a contribution from mTORC1 in inflammasome-independent caspase-1 activation, it does show that in MRL*/lpr* MFs, heightened caspase-1 activation and diminished lysosomal acidification require mTORC2.

In B6 MFs, caspase-11 localizes to vesicles containing IgG-IC and activates caspase-1 during their phagocytosis. Thus, we would expect that activated caspase-1 would localize with IgG-ICs, an event that might be impaired in lupus-prone MRL/lpr MFs. Upon phagocytosis of IgG-ICs, FLICA staining colocalizes with IgG-ICs in B6 MFs indicating that the activation of caspase-1 is localized to vesicles containing IgG-ICs (Fig 3H). In MRL/*lpr* MFs, the colocalization of activated caspase-1 with IgG-ICs is reduced 3-fold (Fig 3H-I). The mislocalization of activated caspase-1 following phagocytosis of ICs does not completely inhibit its activity as MRL/*lpr* MFs have heightened basal levels of activated caspase-1 (Fig. 3E) and

increased inflammasome formation as a consequence of diminished lysosomal maturation (*169*). Consistent with a dependence on mTOR, treatment of MRL/*lpr* MFs with Torin1 restored the localization of activated caspase-1 to levels comparable to B6 (Fig 3H-I). This demonstrates that the activation of caspase-1 is localized to phagocytosed IgG-ICs and that mTOR activity in MRL/*lpr* MFs prevents caspase-1 activation.

To determine whether the activation of caspase-1 is necessary for lysosomal acidification, we inhibited caspase-1 with VAD FMK and quantified the relative pH of MFs stimulated with IgG-ICs. We found that inhibiting caspase-1 reduced acidification of B6 MFs (Fig 3J). The role for caspase-1 activity in lysosomal acidification was not dependent on the formation of an inflammasome because MFs from ASC-deficient mice acidified to levels comparable to B6. This demonstrates that in normal mice, MFs require caspase-1 to fully acidify lysosomes, and that caspase-1 activation is independent of inflammasome formation.

The process of lysosomal maturation is complex; however, a role for mTOR and caspases-1 this process has never been appreciated. If caspase-1 activation were necessary for lysosomal maturation, inhibiting caspase-1 would prevent acidification in B6 MFs. We found that B6 MFs treated with FAM-YVAD-FMK and stimulated with IgG-ICs failed to fully acidify (Fig 3J). This demonstrates that caspase-1 activation is necessary for lysosomal acidification. Further, caspase-1 activation was not dependent on inflammasome formation as MFs from ASC-deficient mice acidified to similar levels as B6. Therefore, inflammasome-independent activation of caspase-1 is necessary for lysosomal acidification in normal MFs. Inhibiting caspase-1 in B6 MFs created a phenotype much like that seen in MRL/*lpr* MFs. Coupled with our findings that chronic activation of mTOR in MRL/*lpr* MFs results in diminished lysosomal acidification and their inability to activate or properly localize caspase-1 with vesicles containing

IgG-ICs, the data indicate a previously unappreciated role for caspase-1 in lysosomal degradation.

Caspase-1 mediated cleavage of Rab39a is necessary for lysosomal maturation

Rab GTPases associate with specific membranes and are integral in the phagocytosis, vesicular trafficking, and exocytosis pathways. The function of Rab39a is relatively uncharacterized; however it localizes to phagosomes and functions in lysosomal acidification (*188*). Furthermore, Rab39a contains a caspase-1 cleavage site and *in vitro* and *in vivo* studies have shown that caspase-1 cleaves Rab39a and that the expression of Rab39a is necessary for the secretion of IL1-β (*189*). Thus, it is possible that phagolysosomal acidification requires caspase-1 to cleave Rab39a. To test this, we stimulated B6 and MRL/lpr BMMFs with IgG-ICs, and then immunoprecipitated Rab39a. B6 MFs showed 9.6-fold more Rab39a N-terminal cleavage product compared to MRL/*lpr* (Fig 4A-C). Although we could detect endogenous full length Rab39a, the detection of the N-terminal cleavage product was weak, while the C-terminus was undetectable. To resolve this, we are currently designing a plasmid to overexpress Rab39a in BMMFs. We will overexpress HA- and/or Flag-tagged (N- and C-terminus respectively) Rab39a in MFs to easily identify both cleavage products and full length Rab39a. We also will generate a mutated form of Rab39a where the putative cleavage site (Asp^{148}) was replaced by Ala (Rab39aD148A). Finally, we will also generate both the Rab39a N-terminal and C-terminal cleavage products to determine if overexpression of either cleavage product is sufficient in restoring lysosomal acidification in MRL/*lpr* MFs.

While the new plasmids are being generated, we were able to compare the wild type Rab39a to the Rab39aD148A by transducing immortalized (v-Myc) B6 MFs and quantifying acidification. Immortalized B6 MFs expressing wild type Rab39a acidified normally with a 15%

decrease in pH following IgG-IC exposure (Fig 4c). In contrast, MFs expressing Rab39aD148A only experienced a 2% decrease in pH indicating that they were unable to acidify the lysosome in the presence of IgG-ICs. This demonstrates that the cleavage of Rab39a at the caspase-1 cleavage site is a necessary step in lysosomal acidification. The new plasmids will allow to further probe the mechanism for Rab39a and lysosome acidification in BMMFs from B6 and MRL/*lpr* MFs.

Discussion

The process of lysosomal maturation and acidification is important in destroying pathogens and clearing cell debris internalized by phagocytosis. This study defines a previously unappreciated role for actin-dependent caspase-1 activation in lysosomal acidification. We show that MFs initiate lysosomal maturation when phagocytosed IgG-ICs (cell debris bound by autoantibody) enter the cell through FcγRs. FcγR-mediated signal transduction activates and localizes mTOR to the plasma membrane (Fig. 5, **1**) promoting heightened phosphorylation of cofilin (Fig. 5, **2**). In its un-phosphorylated state, cofilin associates with F-actin (Fig. 5, **3**), which recruits and activates caspase-11 (Fig. 5, **4**). This in turn promotes the activation of caspase-1 (Fig. 5, **5**) and cleavage of Rab39a (Fig. 5, **6**), a critical event in lysosomal maturation. Thus, the polymerization of actin is key in phagocytic cup formation and internalization of cargo while cofilin and the depolymerization of actin are critical in the maturation of the phagosome and lysosomal acidification.

An unexpected step in the sequence of events leading to lysosomal maturation is the activation of caspase-1, an enzyme normally associated with inflammasome formation and innate immune responses. Activated caspase-1 cleaves pro-IL-1β and induces pyroptosis. This study shows that caspase-1 also plays a central role in lysosomal maturation. The activation of

caspase-1 in lysosomal maturation is independent of inflammasome formation because mice deficient in ASC undergo normal lysosomal maturation and acidification (Figure 3). This reveals that pyroptosis and phagosomal maturation, two distinct cellular mechanisms, are the consequence of caspase-1 activation. However, it raises the question of how caspase-1 activation in B6 MFs internalizing IgG-ICs induces the maturation of lysosomes without promoting cell death. One possibility is that varying levels of caspase-1 execute different functions. For example, low levels of active caspase-1 might promote phagosomal maturation, while high levels may be required for pyroptosis. In support of this graded caspase response, other studies have shown that low levels of caspase-3 or caspase-8 activation can regulate autophagic cell death, the differentiation and proliferation of T and B cells, and the maturation of DCs, while high levels of activation promote apoptosis (*190*). A second influence on the outcome of caspase-1 activation may be location. Restricting activated caspase-1 to maturing phagosomes (Figure 3) might require that caspase-1 act only on Rab39a localized to endosomal and lysosomal structures. In contrast, localizing gasdermin D near the developing inflammasome (and not the phagosome) directs the cleavage by caspase-1 or caspase-11 during pyroptosis (*191, 192*).

Why would caspase-1 be linked to basic cellular functions such as lysosomal maturation when elevated caspase activation results in irreversible cell death? One possibility is that recruitment of caspase-1 to the phagosomal membrane is an evolutionary mechanism to heighten the "pyroptotic potential" when the integrity of the phagosomal membrane is compromised. Intracellular pathogens that escape the phagosome activate caspase-1 (*193*) and caspase-11 (*194*). Thus, localizing caspase-1 in close proximity to the phagosome may promote efficient immune activation if pathogens breach the lysosomal membrane. In this scenario, cytosolic

sensors act to protect the host. This example illustrates how two distinct functions of caspase-1 (lysosomal maturation and pyroptosis) might have co-evolved as a means to safeguard the host during infection.

An unfortunate consequence of this putative host survival mechanism could be that environmental or genetic defects that disrupt lysosomal maturation, such as heightened mTORC2 activation as seen in lupus-prone MRL/*lpr* MFs, compromises the integrity of the phagosomal membrane allowing nuclear antigens to leak into the cytosol (*169*). This allows cytosolic sensors, such as AIM2, to recognize nuclear antigen and promote pyroptosis and innate immune activation against self-antigens (*169*). Thus, the inability to mature the lysosome in SLE may represent an example of how a mechanism intended to safeguard the host during infection turns against the host leading to immune dysregulation and autoimmune disease. This also reveals that defects in basic cellular mechanisms may underlie the defects in the immune system associated with SLE. Impaired lysosomal maturation can drive chronic activation of the internalizing receptors (ie: FcγRI) coupled with the acute activation of intracellular innate receptors (ie: cytosolic sensors, TLRs) that depending on the cell type can drive the pathologies associated with disease. For example, diminished lysosomal maturation in pDCs could heighten secretion of IFNα (*134*), while diminished lysosomal maturation in macrophages and neutrophils may heighten cell death (*153*). This in part might explain some of the more complex phenotypes seen during autoimmunity.

Our study uses a lupus model to elucidate key steps in lysosomal maturation. MFs from lupus-prone MRL/*lpr* mice fail to fully mature lysosomes and the un-degraded IgG-ICs remain bound to FcγRs and recycle back to the cell membrane (Fig. 5, **7**). Accumulation of un-degraded IgG-ICs promotes BAFF secretion and lupus nephritis (*37*). It also prolongs the length of time

IgG-ICs reside in the endocytic pathway inducing TLR7 and TLR9 activation and autoantibody secretion (*37, 169*). Prolonged residency in the phagosome and heightened levels of incoming cargo permeabilize the phagosomal membrane allowing nuclear antigens and autoantibody from the IgG-ICs to leak into the cytosol activating cytosolic sensors including AIM2 and TRIM21 heightening IFNα levels (*169*). Mechanistically the chronic activation of FcγRI heightens mTORC1/C2 activation, and chronically mislocalizes mTOR at the plasma membrane increasing the levels of p-cofilin (Fig. 5, **2**), diminishing the association of cofilin and caspase-11 with F-actin and preventing F-actin depolymerization and caspase-11 activation (Fig. 5, **8**). As a consequence caspase-1 is not activated, and does not associate with vesicles containing IgG-ICs (Fig. 5, **9**). This limits the cleavage of Rab39a (Fig. 5, **10**), thereby preventing phagosomal maturation. Thus, diminished lysosomal maturation in MFs from lupus-prone MRL/*lpr* mice creates a vicious cycle wherein undegraded IgG-ICs bound by FcγRs, recycle back to the cell surface leading to chronic activation of mTOR and continued loss of lysosomal maturation. These data identify a previously undescribed signaling pathway regulating lysosomal maturation and revealing potential therapeutic targets in restoring the clearance of apoptotic debris in SLE.

Materials and Methods

Mice

C57BL/6 (B6) and MRL/MpJ-*Tnfrs6*^{lpr}/J (MRL/*lpr*; JAX mice Stock # 000485) colonies were maintained in an accredited animal facility at University of North Carolina at Chapel Hill (UNC-CH). *Casp1/11*$^{-/-}$/C57BL/6 (*195*), *Casp11*$^{-/-}$/C57BL/6 (*196*), *pycard*$^{-/-}$/C57BL/6 (*197*) mice were obtained from Dr. Edward Miao. We generated FcγRI$^{-/-}$MRL/*lpr* mice by backcrossing FcγRI$^{-/-}$/C57BL/6 mice to MRL/*lpr* mice for 10 generations.

Reagents

Antibodies specific for CD11b were purchased from BD Biosciences, pS6, S6, pAKT (ser), pAKT (thr), AKT, pAMPK, AMPK, mTOR, cofilin, p-cofilin, caspase-11, and tubulin from Cell Signaling, goat anti-rabbit IgG and rabbit anti-goat IgG from Molecular Probes, and Rab39 from ProteinTech. Concanamycin A was purchased from Sigma-Aldrich, Antibodies specific to Smith (Sm; 2.12.3), nucleosome (PL2-3) and CD16/32 (2.4G2) were purified from hybridoma culture supernatant using protein G-Sepharose (GE Healthcare) then left unlabeled or conjugated with Alexa fluor according to the manufacturer instructions (Molecular Probes). Fluorescent molecule LysoSensor Yellow/Blue was purchased from Molecular Probes and FAM-FLICA caspase-1 assay kit from ImmunoChemistry Technologies. LI-COR blocking buffer and IRDye680- and IRDy800-conjugated antibodies (anti-rabbit, anti-mouse, anti-goat) were purchased from LI-COR Biosciences.

Bone Marrow-derived MF (BMMF) cultures

Single-cell suspensions of bone marrow were prepared from the tibias and femurs of C57BL/6 mice. Mononuclear cells were isolated using Lympholyte Separation Medium (CEDARLANE Laboratories, Burlington, ON) plated in 60 mm petri dishes with 6 mL macrophage differentiation media (DMEM with 10% FBS, 10% L-cell supernatant, 1 mM sodium pyruvate, 50 μg/mL gentamicin, 100 μg/mL Pen/Strep, 2mM L-glutamine, 50 nM β-ME. After the overnight culture (37°C, 5% CO_2), non-adherent cells were plated into non-tissue culture treated 100 mm petri dishes (0.75-1 mL cells/petri dish) with 7 mL fresh macrophage differentiation media and incubated for 6 days to promote macrophage differentiation. On day 4, culture medium was replenished with an additional 5 mL of macrophage differentiation media.

The resulting bone marrow derived macrophages were removed from the dish by washing with ice cold PBS. BMMF cultures were 98% $CD11b^{+}$, $I\text{-}A^{lo}$, and $B7.2^{lo}$.

Formation of Immune Complexes

Apoptotic debris-containing immune complexes (IgG-IC): Single-cell suspensions of thymocytes were prepared from 5-8 week mice, irradiated (600 rads) and cultured 16-18 hours in 10 mL PBS (37°C, 5% CO_2). Apoptotic thymocytes were centrifuged for 5 minutes (350 x g) and the supernatant containing apoptotic debris was incubated with autoantibodies (2.12.3 or PL2-3) on ice for 30 min (6.67 μg Ab/1 mL supernatant). Immune complexes were pelleted (160,000 x g) at 4°C for 45 min. Pelleted ICs were resuspended in 250 μL R10 media (RPMI with 10% FBS, 1 mM sodium pyruvate, 50 μg/mL gentamicin, 100 μg/mL Pen/Strep, 2mM L-glutamine, 50 nM β-ME).

Fluorescent Microscopy

All confocal microscopy was conducted using a Zeiss 710 confocal microscope with a 63 × 1.4 NA (oil) PLAN APO lens and Zeiss Zen software. Data were analyzed using ImageJ. mTOR localization: BMMFs were fixed with 2% paraformaldehyde, then incubated at 4°C for 15 min. Cells were blocked in 2.4G2 for 30 min at 4°C, stained with an anti-mTOR antibody and Hoechst 33342 (1 μg/ml) in permeabilization buffer (PBS with 0.05% Saponin and 0.5% BSA) for 30 min at 4°C. Cells were washed again and stained with anti-CD11b in FACS media (PBS with 2% FBS, 0.02% NaN_3) for 30 min at 4°C, washed, resuspended in FluorSave and loaded onto coverslips for microscopic imaging. The membrane localization of mTOR was quantified by calculating the Mander's coefficient of colocalization (ratio of colocalized pixels/total fluorescent pixels).

Cofilin, p-cofilin, caspase-11 localization: Two hours prior to imaging, BMMFs were incubated (37°C, 5% CO_2) on a glass bottom petri dish (MatTek Corp) in R10 media (rhodamine free RPMI with 10% FBS and pen/strep [as above]). Cells were cultured in the presence of IgG-ICs (apoptotic debris-containing IgG-Alexa 647), fixed at the indicated time points with 2% paraformaldehyde, then incubated at 4°C for 15 min. Cells were blocked in 2.4G2 for 30 min at 4°C, stained with Alexa 568 phalloidin, or an anti-cofilin, p-cofilin, caspase-11 antibody, and Hoechst 33342 (1 μg/ml) in permeabilization buffer (as above) for 30 min at 4°C. Cells were washed again, stained with goat anti-rabbit IgG-Alexa 488 or goat anti-rat IgG-FITC in permeabilization buffer for 30 min at 4°C, washed, and 2 mL of FACs media was added to the dish. The localization of cofilin, p-cofilin, or caspase-11 with actin and IgG-ICs was quantified by calculating the Mander's coefficient of colocalization (ratio of colocalized pixels/total fluorescent pixels).

Active caspase-1 localization: BMMFs were cultured in the presence of apoptotic debris-containing IgG-Alexa647 ICs. FAM-FLICA caspase-1 and Hoechst 33342 (1 μg/ml) was introduced to the cells 20 minutes prior to fixation, washed, and fixed with 2% paraformaldehyde at the indicated time points, then incubated at 4°C for 15 min. Cells were resuspended in FluorSave and loaded onto coverslips for microscopic imaging. The colocalization of active caspase-1 with IgG-ICs was quantified by calculating the Mander's coefficient of colocalization.

Flow Cytometry

All flow cytometry was conducted using an 18-color Becton Dickinson LSR II Flow cytometer and data were acquired using Becton Dickinson FACSDiva 8.0.1 software.

Recycling flow: BMMFs were incubated with 40 μL Alexa488-labeled IgG-ICs in R10 media (as above). To quantify surface bound ICs at 0 hours, phagocytic uptake was impaired by

culturing with IgG-ICs on ice for 2 hours. This was sufficient to allow the ICs to bind to the surface of the cell but not be phagocytosed. For all other time points, cells were incubated (37°C, 5% CO_2) for 2 hours, and then media was replaced to remove all unbound ICs. At indicated time points, cells were blocked in 2.4G2 for 30 min on ice, washed and split into 2 samples. One sample was incubated with an anti-Alexa488 antibody (quenches Alexa488 fluorescence), while the other sample was left in FACS media (as above) for 30 min on ice. Both samples were washed and fixed with 2% paraformaldehyde, and then incubated at 4°C for 15 min. Cells were resuspended in FACS media and the levels of surface IgG-IC were quantified by flow cytometry. External IgG-ICs were calculated by subtracting the Alexa488 quenched sample (internal IgG-ICs) from the unquenched sample (total IgG-ICs).

Ratiometric flow cytometry: BMMFs were incubated (37°C, 5% CO_2) for 2 hours prior to the addition of 40 μL of IgG-ICs in R10 media (as above) and in the presence or absence of indicated drugs. Concanamycin A (20 ng/mL) was introduced to one sample from each cell type as a way to quantify an unacidified cell 2 hours prior to addition of IgG-ICs and left on the cells throughout the experiment. IgG-ICs and LysoSensor (2 mg/mL) were introduced for 30 min, aspirated, and replaced with fresh rhodamine free R10 media. Cells were incubated until indicated time points and analyzed by flow cytometry. A UV laser (355 nm) was used to excite the dye and the MFI from the emission channels (450/20 nm, 585/42 nm) was ratioed to quantify relative pH.

pS6, S6, pAkt (ser), pAkt (thr), Akt, pAMPK, AMPK, mTOR, p-cofilin, cofilin flow cytometry: BMMFs were cultured in the presence or absence of IgG-ICs and fixed at indicated time points with 2% paraformaldehyde, then incubated at 4°C for 15 min. Cells were blocked in 2.4G2 for 30 min at 4°C, washed, and stained with anti-mTOR, -pS6, -S6, -pAkt (ser), -pAkt

(thr), -Akt, -pAMPK, -AMPK, -p-cofilin, -cofilin antibodies in permeabilization buffer (as above) for 30 min at 4°C. Cells were washed again, stained with goat anti-rabbit IgG-Alexa 647 in permeabilization buffer for 30 min at 4°C, washed, and resuspended in FACs media (as above). Relative levels of p-cofilin and cofilin were determined by quantifying the MFI by flow cytometry and ratioing to an isotype control.

Caspase-1 activation: BMMFs were cultured in the presence or absence of IgG-ICs and incubated with FAM-FLICA caspase-1 (5 μM) 20 minutes prior to fixation in FACs media (as above) at room temperature. Cells were fixed in room temperature with 2% paraformaldehyde and transferred to 4°C for 15 min. Cells were resuspended in FACS media and caspase-1 activation was determined by quantifying the MFI using flow cytometry.

Immunoprecipitation and Western Blot

Lysates were prepared by the addition of lysis buffer containing 1% CHAPS or 1% NP40, 150 mM NaCl, 10 mM Tris (pH 7.5), 2 mM sodium orthovanadate, 1 mM PMSF, 0.4 mM EDTA, 10 mM NaF, and 1 μg/ml each of aprotinin, leupeptin, and α1-antitrypsin to cell pellets. Lysates were held on ice for 10 min followed by the removal of particulate material by centrifugation at 12,000 × *g* for 10 min at 4°C. Lysates were then by 10% (S6 and Akt signaling) or 15% (Rab39a) SDS-PAGE. Separated proteins were transferred to Immobilon-FL membranes. Membranes were blocked in LI-COR Blocking Buffer, then incubated with the various immunoblotting Abs followed by the appropriate fluorophore-conjugated secondary Abs. Immunoreactive proteins were detected using a LI-COR Odyssey infrared imaging system with Odyssey 3.0 software.

Figures

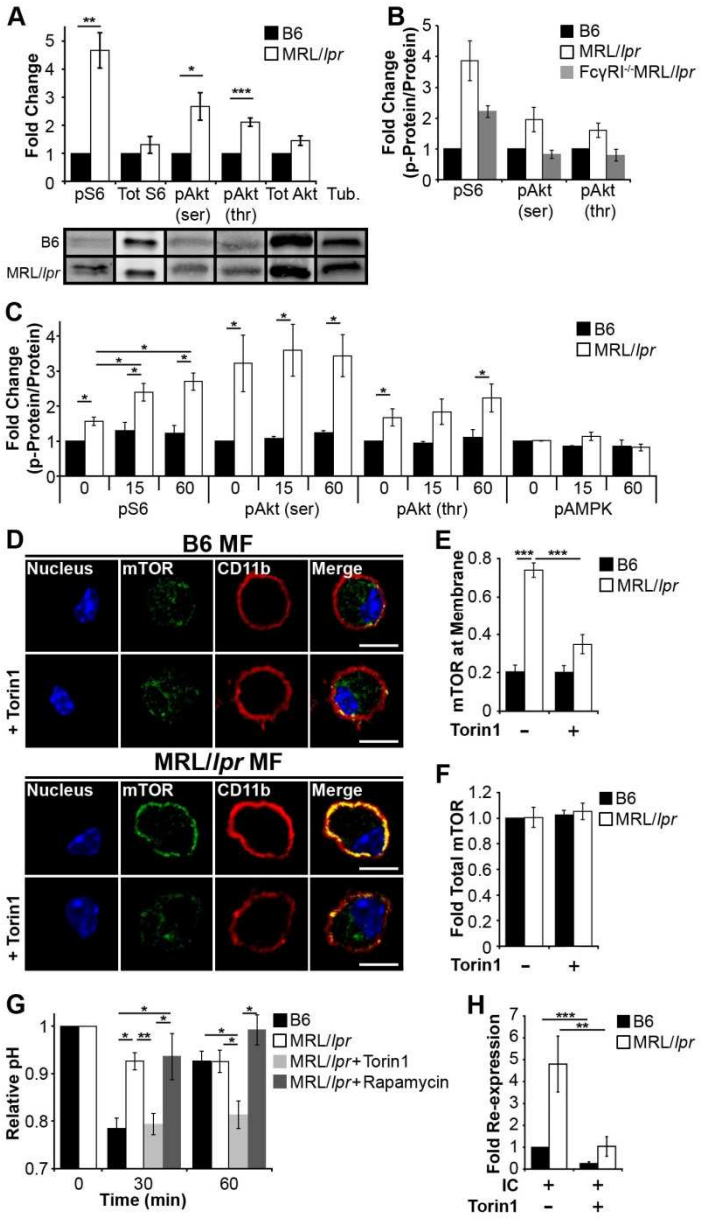

Figure 1. Heightened and mislocalized mTOR activity impairs lysosomal maturation in lupus-prone MFs. Cell lysates from unstimulated BMMFs (1-1.5x10^6 cells) were quantitated by immunoblot for the indicated proteins; 4 experiments, 4 mice (**A-B**). A representative blot is shown with densitometry quantification (A) and densitometry quantification of phospho-proteins normalized to total protein (B). BMMFs were stimulated with IgG-ICs and analyzed for the indicated signaling effectors over time using flow cytometry 5 experiments, 3-6 mice (**C**) Phospho-proteins were normalized to total protein. BMMFs were stimulated with IgG-ICs ± Torin1 (250 ng/mL), and then examined by confocal imaging for the location of mTOR within the cell (Bar = 5 μm); 2-3 experiments, 2-3 mice, 10-29 cells (**D-E**), and by flow cytometry for the total levels of mTOR; 3 experiments, 3 mice (**F**). BMMFs were stimulated with IgG-ICs ± Torin1 (250 ng/mL), or ± rapamycin (100 ng/mL) and assessed for lysosomal pH by ratiometric flow cytometry, 10 experiments, 10-12 mice (**G**). BMMFs were stimulated with fluorescently-

tagged IgG-ICs ± Torin1 (250 ng/ml), for 72 hours, and then assessed for surface fluorescence by flow cytometry; 5-6 experiments, 5-6 mice (**H**). Error bars=SEM. Statistical analysis for all panels used Student *t* test, *$p \leq 0.05$, **$p \leq 0.01$, ***$p \leq 0.001$.

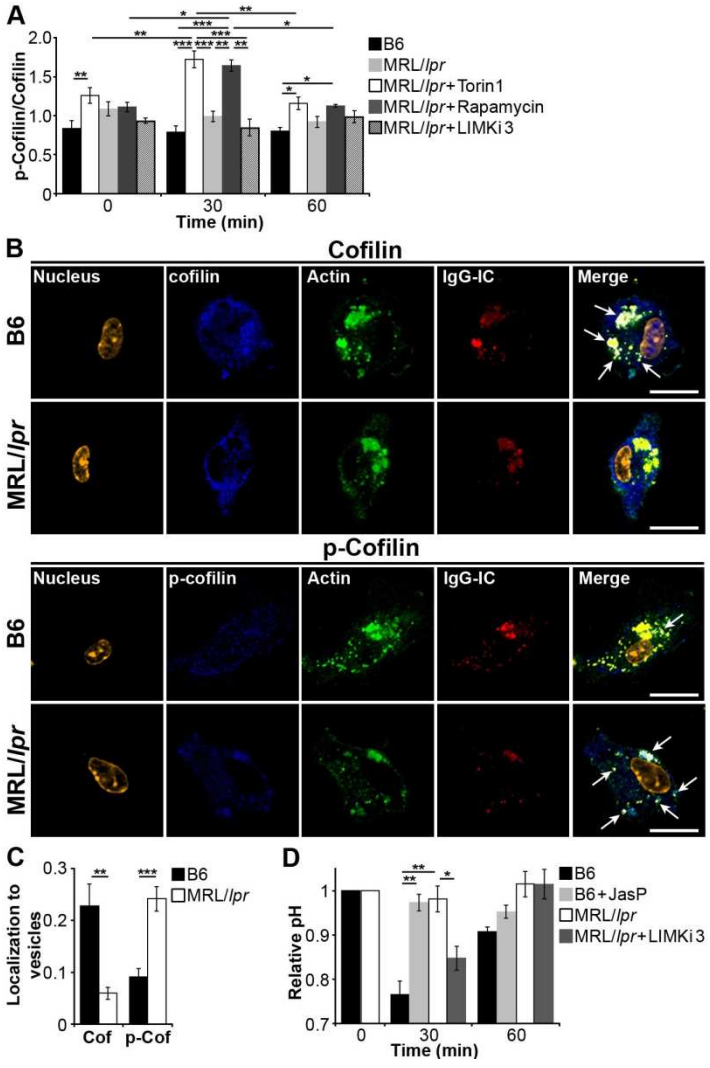

Figure 2. Heightened mTOR activity impairs lysosome maturation by driving the phosphorylation of cofilin. BMMFs were stimulated with IgG-ICs ± Torin1 (250ng/mL), rapamycin (100 ng/mL), or LIMKi 3 (3 μM) and analyzed at indicated time points for levels of p-cofilin by flow cytometry; 10 experiments, 3-10 mice (**A**). p-cofilin levels are normalized to total cofilin levels. BMMFs were stimulated with IgG-ICs for 15 minutes and examined by confocal imaging for the localization of p-cofilin and cofilin with actin and IgG-ICs, (Bar = 5 μm); 3 experiments, 3 mice, 13-14 cells (**B-C**). BMMFs were cultured with jasplakinolide (2 μM) or LIMKi 3 (3 μM) for one hour, and then stimulated with IgG-ICs and assessed for lysosomal pH by ratiometric flow cytometry, 4 experiments, 4 mice (**D**). Error bars=SEM. Statistical analysis for all panels used Student *t* test, *$p \leq 0.05$, **$p \leq 0.01$, ***$p \leq 0.001$.

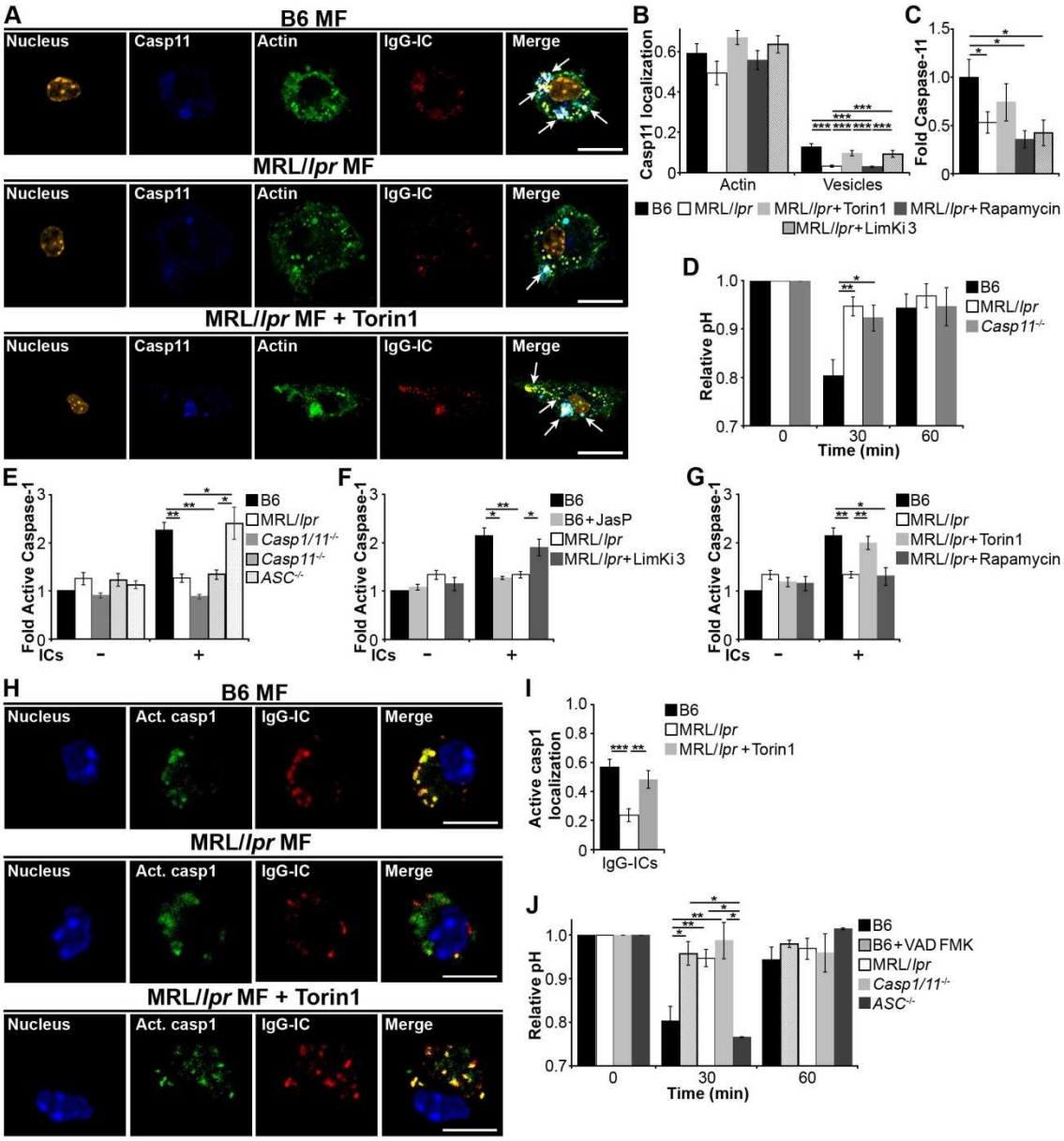

<u>Figure 3</u>: Phosphorylation of cofilin prevents a localized caspase cascade at the phagosome.

BMMFs were stimulated with IgG-ICs for 15 minutes, and then examined by confocal imaging for the localization of caspase-11 with actin and IgG-ICs (Bar = 5 μm) ± Torin1 (250ng/mL), rapamycin (100 ng/mL), or LIMKi 3 (3 μM); 3 experiments, 3 mice, 10-16 cells (**A-C**). BMMFs stimulated with IgG-ICs and assessed for lysosomal pH at indicated time points by ratiometric flow cytometry; 8 experiments, 5-8 mice (**D**). BMMFs from the indicated mice were stimulated with IgG-ICs ± Torin1 (250ng/mL), ± rapamycin (100 ng/mL), ± jasplakinolide (2 μM), or ±

LIMKi 3 (3 μM). Caspase-1 activation was measured by flow cytometry; 6 experiments, 2-6 mice (**E-G**). BMMFs were stimulated with IgG-ICs for 15 minutes, and then examined by confocal imaging for the localization of activated caspase-1 with IgG-ICs (Bar=5 μm); 3 experiments; 3 mice, 30-45 cells (**H-I**). BMMFs stimulated with IgG-ICs and assessed at indicated time points for lysosomal pH by ratiometric flow cytometry; 8 experiments, 2-8 mice (**J**). Error bars=SEM. Student *t* test, *$p \leq 0.05$, **$p \leq 0.01$, ***$p \leq 0.001$.

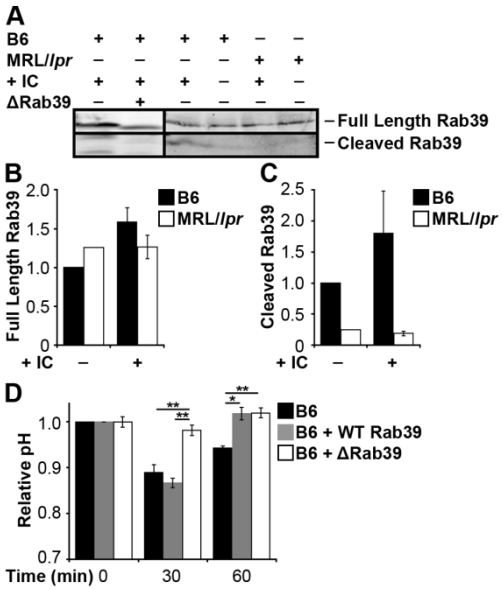

Figure 4. Cleavage of Rab39a by caspase-1 is integral for lysosomal maturation. BMMFs were stimulated for 1 hour with IgG-ICs. Following Rab39a immunoprecipitation (13-15x10^6 cells), Rab39a protein levels were immunoblotted (**A**) and full length and cleaved Rab39a was quantitated by densitometry; 3 experiments, 3 mice (**A-C**). B6 v-Myc MFs were transduced with indicated retroviral constructs. Once constructs were stably expressing, MFs were stimulated with IgG-ICs and MFs expressing GFP were assessed for lysosomal pH at indicated time points by ratiometric flow cytometry; 3 experiments (**D**). Error bars=SEM. Student *t* test, *$p \leq 0.05$, **$p \leq 0.01$, ***$p \leq 0.001$.

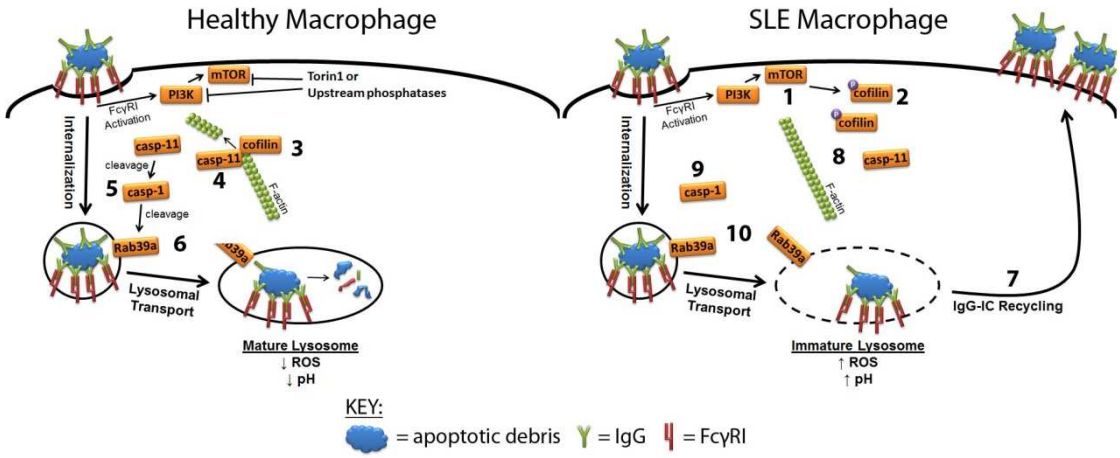

Figure 5. Signaling pathway regulating Rab39a mediated lysosomal maturation in lupus-prone and healthy MFs.

Supplemental Figures

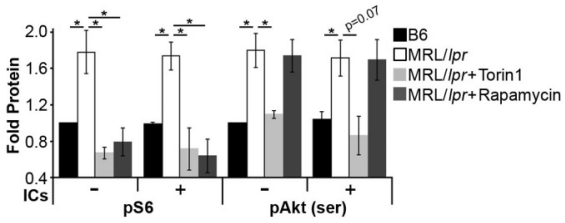

Fig. S1. Torin1 inhibits mTORC1/C2 while rapamycin inhibits mTORC1. BMMFs were stimulated with IgG-ICs for 60 minutes and analyzed for the indicated signaling effectors using flow cytometry; 3 experiments, 3 mice. Error bars=SEM. Student *t* test, *$p \leq 0.05$, **$p \leq 0.01$, ***$p \leq 0.001$.

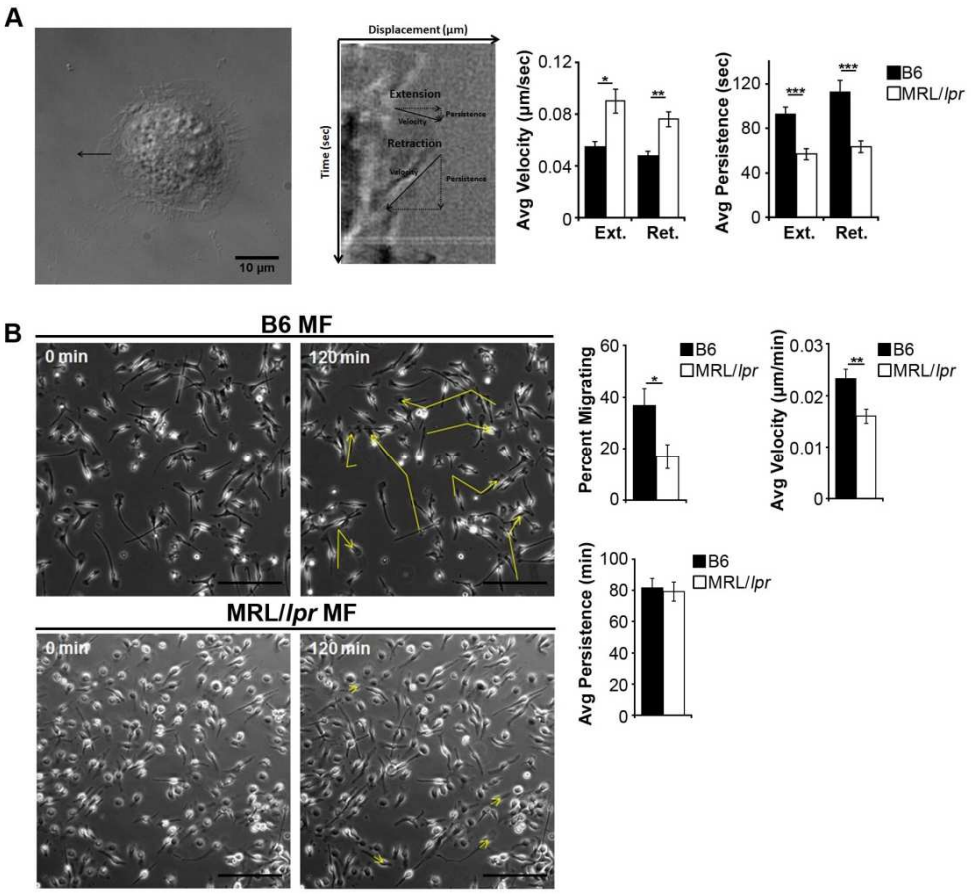

Fig. S2. MRL/*lpr* MFs have impaired membrane ruffling and decreased migration. BMMFs were plated onto glass coverslips and after 48 hours where imaged for membrane ruffling (Bar = 10 μm) (**A**). A kymograph was generated for each cell and the persistence and average velocity for membrane extension and retraction was quantified; 3 experiments, 3 mice, 37-39 cells. BMMFs were plated onto fibronectin coated glass coverslips and after 24 hours where imaged for MF migration (Bar = 130 μm) (**B**). The percentage of migrating cells was quantified per field of view over a 2 hour time course. Also, the average velocity and persistence of migration was quantified for each migrating cell; 3 experiments, 3 mice, 24-30 cells. Error bars=SEM. Student *t* test, *$p \leq 0.05$, **$p \leq 0.01$, ***$p \leq 0.001$.

CHAPTER 4: Discussion

With the advancement of genetics, genome wide association studies (GWAS) were thought to be the key to identifying the underlying mechanisms to autoimmune diseases. It's based on the common disease-common variant hypothesis where the allelic frequency of variants that cause common diseases are shared (common) across patients (*198, 199*). Like many other autoimmune diseases, the SLE GWAS identified multiple polymorphisms, many of which had a low penetrance with an odds ratio less than 2 (*160, 200-212*). One possible interpretation is that the acquisition of polymorphisms is additive and that acquiring multiple polymorphisms with a low odds ratio surpasses a predetermined threshold resulting in SLE pathogenesis. They propose that larger studies and further parsing of the data would yield more insights into disease. Another possibility is that the results verify that the common disease-common variant hypothesis does not apply to complex human diseases (*213*). Instead, disease-causing alleles might be rare with many allelic variants leading to common mechanistic defects. For example, we see that 70-80% of flaring SLE patients accumulate IgG-ICs on the surface of PBMCs. In MRL/*lpr* mice, this accumulation is the result of heightened mTOR activity leading to impaired lysosomal maturation. In SLE patients, there are many possible variants that can alter phagocytosis, vesicular trafficking, and lysosomal function that would lead to the same impaired degradation of IgG-ICs and accumulation at the membrane. Therefore in the context of complex human diseases identifying common mechanisms underlying disease pathology will be more productive than high-powered GWASs.

Patients who have been diagnosed with an autoimmune disease tend to have an increased risk of acquiring secondary autoimmune diseases. For example in patients diagnosed with SLE, overlapping autoimmune diseases such as diabetes (*156*), rheumatoid arthritis (*157*), and Sjögren's syndrome (*158*) are common. This suggests that there are fundamental defects/mechanisms in autoimmunity that permeate multiple diseases in addition to modulating factors that are unique to specific autoimmune diseases. My thesis project has identified that lupus-prone MFs fail to properly mature the lysosome and as a result they do not fully acidify. Therefore phagocytosed IgG-ICs are not degraded and accumulate on the cell membrane. The accumulation was not unique to the MRL/*lpr* background as genetically unrelated models of lupus (NZM2410) also accumulated high levels of IgG-ICs. Furthermore the accumulation of IgG-ICs occurs in other models of autoimmunity including diabetes (NOD) and arthritis (K/BxN). Since these murine models are genetically unrelated to lupus, impaired lysosomal degradation of internalized cargo (ie: IgG-ICs) could be a fundamental defect in autoimmunity, while the specific antigen contained in the cargo would modulate disease.

In a pilot study I tested whether the impaired lysosomal degradation of IgG-ICs is fundamental to autoimmunity, while the accumulating antigen is unique to specific diseases. If a lysosomal defect underlies diabetes then insulin could be the antigen accumulated on the surface since the antigen is specific to beta cells and autoantibodies are produced against insulin during autoimmunity. We analyzed splenic MFs from diabetic NOD mice ($\geq$ 26 weeks; blood glucose levels $\geq$ 500 pg/dL) for accumulation of IgG, Sm, and insulin. Even though IgG and Sm was elevated and punctate on the surface of diabetic MFs, there was no detectable accumulation of insulin on the surface of the cells. During diabetes it's been demonstrated that the profile of autoantibodies changes over time and it's possible that insulin-containing ICs are relatively low

when the mice are fully diabetic (blood glucose level ≥ 500 pg/dL). In a separate study, I quantified IgG and Sm levels on the surface of PBMCs from NOD mice at different blood glucose levels. Pre-diabetic mice (blood glucose levels < 100 pg/dL) had Sm levels comparable to B6 on the surface of monocytes. As blood glucose levels rose, Sm on the surface of the monocytes also increased. Interestingly, IgG levels on the surface of monocytes were bimodal with the highest in pre-diabetic and fully diabetic mice. This could suggest that IgG-ICs in fully diabetic mice could consist of a higher proportion of apoptotic debris, while pre-diabetic mice could have IgG-ICs with a higher proportion of diabetogenic antigens. Therefore, hematopoietic cells from pre-diabetic mice may need to be used to identify accumulated insulin (or other diabetogenic antigens) on the cell surface. Furthermore, if impaired lysosomal degradation underlies multiple autoimmune disease, it's possible that the antigen underlying the disease can evolve as the autoimmunity progresses.

Nuclear antigens accumulate on the surface of multiple hematopoietic cells (B cells, T cells, MFs, and DCs) suggesting that the lysosomal maturation defect affects multiple cell types. In MFs and DCs the accumulated nuclear antigen was in the form of IgG-ICs bound primarily to FcγRI and FcγRIV. B cells have one FcγR (FcγRIIb) and studies utilizing FcγRIIb deficient mice demonstrated that FcγRIIb only accounts for 10% of the nuclear antigen that accumulates on B cells. The BCR is not a likely candidate for how nuclear antigen is displayed since all the B cells in MRL/*lpr* mice seem to accumulate nuclear antigen and it's unlikely that every BCR shares an affinity for nuclear antigen. I hypothesized that nuclear antigen accumulate on B cells due to mislocalized TLR7 and TLR9 (and in humans, TLR8) on the surface of the cell as a result of impaired lysosomal maturation. TLR7 and TLR9 traditionally localize to the phagolysosome to interact with their ligands and signal intracellularly (*214*). Prior to the activation of the BCR,

endosomal TLRs are localized to the ER and have limited access to ligand, which prevents aberrant TLR activation. In a pilot study we found lupus-prone B cells do not acidify their lysosomes. This suggests two possible mechanisms that could drive intracellular TLRs to the cell membrane and allow them to bind exogenous nuclear antigen. First, apoptotic debris is internalized and trafficked to the phagolysosomal compartment where the nuclear antigen binds TLRs. Since, the lysosome does not acidify, the nuclear antigen does not get degraded and the nuclear antigen bound to intracellular TLRs is recycled back to the cell membrane much like we saw in MFs where IgG-ICs bound by FcγRs are recycled. The second possibility is that activation by cytokines (BAFF, IFNα) and/or the BCR promotes TLR translocation to the phagolysosome. Since the phagolysosome does not acidify, empty TLRs can traffic to the cell membrane where they can bind to extracellular nuclear antigen. In either scenario, it's possible that the TLRs bound to nuclear antigen will be able to signal from the membrane which brings up an interesting situation. Autoreactive B cells are either deleted or tolerized based on BCR specificity. Therefore in peripheral B cells that are not tolerized, the BCR acts as the gate that spatially separates universal PAMPs (ie: DNA, RNA) from intracellular innate receptors. If intracellular TLRs localize to the membrane and bind their ligands to elicit downstream signaling, this would essentially bypass BCR specificity and allow B cells to activate indiscriminately. It's been demonstrated that TLR7 and TLR9 play an important role in SLE pathogenesis but most of these studies were done with RF B cells and ICs, therefore the TLR activation was only addressed in the context of an autoreactive B cell (*90, 215*). As a result, there has been no mechanistic explanation how intracellular TLRs remain chronically activated during autoimmunity in non-autoreactive B cells. Impaired lysosomal maturation inducing intracellular TLRs to the cell membrane may provide a mechanism for the breakdown in B cell

tolerance through chronic activation of mislocalized/surface TLR7 and TLR9. Current studies in the lab have identified that impaired lysosomal acidification drives heightened intracellular TLRs to the membrane, TLR9 is capable in binding DNA at the membrane, and B cells from MRL/*lpr* mice and SLE patients have heightened levels of TLR7 and TLR9 on the surface of the cell.

While the mislocalization of intracellular TLRs may underlie the accumulation of nuclear antigens in B cells, this does not seem to be the case in T cells. Furthermore, we have been unable to identify any receptors critical in the accumulation of nuclear antigens on T cells. T cells are unique because the other hematopoietic cells (B cells, MFs, and DCs) accumulate low levels of nuclear antigen on the surface, but T cells do not. Only lupus-prone T cells accumulate nuclear antigen. This suggests that the mechanism for the accumulation of nuclear antigens on T cells is only present during autoimmunity. Furthermore the other hematopoietic cells are antigen presenting cells and are capable of internalizing antigen via FcγRs or the BCR to process and present to T cells. However, T cells have never been described to possess a similar internalization capacity. It's possible that lupus-prone T cells express a receptor during the disease state that is not present in healthy T cells. Another possibility is that the T cells accumulate nuclear antigen through a process called trogocytosis, which involves the transfer of plasma membrane fragments from one cell to another. Trogocytosis allows recipient cells to acquire molecules that they do not usually express and/or strips donor cells of molecules altering their function (*216-220*). This interaction has been demonstrated to occur during MHC presentation of peptides on APCs to the cognate TCR on T cells (*217, 221, 222*). Therefore, during autoimmunity when a DC has accumulated high levels of nuclear antigens on the surface, when it presents processed peptide antigens through the MHC to a T cell, the T cell is able to capture the entire MHC-peptide complex along with other molecules on the membrane of the

DC. Since there are heightened levels of nuclear antigen on lupus-prone DCs compared to healthy, there is a higher probability that nuclear antigen will be transferred to the cognate T cell during antigen presentation, which may explain why healthy T cells do not show accumulated nuclear antigen. It's possible that the nuclear antigen and/or FcγRs are able to elicit downstream signaling in T cells, which could alter its activation state but further experiments will need to be performed to test this hypothesis.

The observation that IgG-ICs recycle back to and accumulate on the surface of the cell is might be a normal cellular defense mechanism that is being applied incorrectly. There is a subset of pathogens that upon phagocytosis are able to either escape the phagosome or halt phagosomal maturation so that they can replicate intracellularly. In this scenario, it would be the in the host cell's best interest to recycle the pathogen back to the surface of the cell. First, intracellular pathogens typically utilize the host's intracellular proteins for nutrients and replication. Therefore by recycling the pathogen back to the cell surface it could impair the pathogen's replication by spatially restricting it to the extracellular region. Furthermore, the recycled pathogen could still be attached to the receptors that were critical in phagocytosis which would restrict the pathogen's mobility. Second, the accumulated pathogen on the surface of the cell could be used to initiate an immune response. The accumulated pathogen on the surface of the cell creates a repeating high avidity substrate to crosslink the BCR on nearby B cells and initiates antibody secretion independent of T cell help. If the accumulated pathogen on a host cell is recognized by a MF and it is unable to engulf the entire pathogen-host cell complex, this could initiate frustrated phagocytosis where a synapse would be formed between the host cell and the MF. The MF would then release ROS, anti-microbial peptides, and proteolytic enzymes to destroy the pathogen-host cell complex. Finally, the accumulated pathogen on the surface of

the cell could act as a danger signal that the host cell is potentially infected. This could trigger nearby neutrophils to degranulate and kill the host cell, thereby preventing replication of the pathogen. Lupus-prone MFs are unable to degrade phagocytosed IgG-ICs and this could be interpreted as a pathogen hindering lysosomal maturation. As a result, IgG-ICs are recycled to the membrane which places high levels of nuclear antigen on the surface of the cells, priming an immune response against self-antigens.

One unpublished experiment that I conducted might support this hypothesis. B6 MFs that were cultured with live E. coli killed and degraded the bacteria and recycled only small amounts of LPS back to the cell surface at 12 hours and 72 hours post-infection (0.74-fold). In contrast MRL/*lpr* MFs were unable to efficiently kill or degrade the bacteria and continuously accumulated LPS on the surface of the cell out to 72 hours (6.4-fold). While these results are consistent with the recycling of pathogens as a cellular defense mechanism, further studies will need to be conducted to solidify these claims. Currently it's unknown whether the LPS seen on the surface of the cells was whole or pieces of partially degraded bacteria. It would also be interesting to infect B6 MFs with a more virulent strain of *E. coli* (one that is resistant to lysosomal degradation or prevents this process) to see if this induces heightened recycling of LPS to the surface.

If we assume that this mechanism exists in cells as a means of combating intracellular pathogens, it may also play an equally important role in establishing tolerance for B cells. As mentioned previously, the intracellular bacteria might be localized to the cellular membrane to spatially restrict it from intracellular molecules necessary to its replication. In this model, the receptor would still be crosslinked by the pathogen therefore the receptor would need to be modified in order to prevent reinternalization. This could be achieved by ITAMi formation or

the conversion of a dually phosphorylated ITAM to monophosphorylation which prevents Syk activation and downstream signaling. Therefore, when FcγRI internalizes IgG-ICs and the lysosome cannot degrade the cargo, this results in prolonged ITAM activation which could supply a signal to dephosphorylate one of the ITAM residues so that when the receptor recycles back to the membrane it no longer can elicit a downstream signal despite the receptors being crosslinked. Unpublished data demonstrating that recycled IgG-ICs on MRL/*lpr* MFs are severely limited in their dynamics on the membrane and fail to reinternalize (compared to newly bound IgG-ICs) is consistent with this model.

In B cells, this same mechanism can result in anergy. Broadly speaking, there are two forms of tolerance: central tolerance and peripheral tolerance. During central tolerance, when a B cell is identified as autoreactive in the bone marrow, the B cell goes through a series of receptor editing events until either the B cell is no longer autoreactive or the B cell is deleted from the repertoire. In the periphery, when a B cell is chronically stimulated by antigen (typically self-antigens) the B cell becomes anergic where it is no longer active and has heightened basal calcium, p-ERK, and ITAMi formation (*154, 223*). Just as impaired lysosomal degradation of phagocytosed pathogens could lead to prolonged FcγRI signaling and ITAMi formation, chronic activation of the BCR could lead to ITAMi formation and anergy. In short, for a non-autoimmune B cell, recycling of BCRs could induce anergy. It's been commonly thought that a constant supply of exogenous self-antigens is necessary to renew the BCR signaling and maintain anergy, but I propose that once chronic BCR signaling passes a threshold, the BCR recycles back to the membrane bound to its cognate ligand and ITAMi formation is attained. Therefore, once anergy is achieved a source of exogenous ligand is not necessary to maintain anergy because the BCR is already permanently bound to ligand.

REFERENCES

1. G. C. Tsokos, *N Engl J Med* **365**, 2110 (Dec 1, 2011).
2. P. Klemperer, *Ann Intern Med* **28**, 1 (Jan, 1948).
3. A. Kuhn *et al.*, *Arthritis Rheum* **54**, 939 (Mar, 2006).
4. A. L. Hepburn *et al.*, *Ann Rheum Dis* **66**, 1106 (Aug, 2007).
5. E. J. Bardana, Jr., R. J. Harbeck, A. A. Hoffman, B. Pirofsky, R. I. Carr, *Am J Med* **59**, 515 (Oct, 1975).
6. M. Herrmann *et al.*, *Arthritis Rheum* **41**, 1241 (Jul, 1998).
7. L. Ballantine *et al.*, *Pediatr Rheumatol Online J* **13**, 10 (2015).
8. L. F. Fries, W. W. Mullins, K. R. Cho, P. H. Plotz, M. M. Frank, *J Immunol* **132**, 695 (Feb, 1984).
9. C. Y. Hu *et al.*, *Lupus* **18**, 676 (Jul, 2009).
10. Y. Li *et al.*, *Arthritis Res Ther* **11**, R6 (2009).
11. M. C. Pickering, M. Botto, P. R. Taylor, P. J. Lachmann, M. J. Walport, *Adv Immunol* **76**, 227 (2000).
12. H. Yamaguchi *et al.*, *Eur J Immunol* **40**, 1778 (Jun, 2010).
13. R. Licht, C. W. Jacobs, W. J. Tax, J. H. Berden, *Lupus* **10**, 102 (2001).
14. S. W. Tas, P. Quartier, M. Botto, L. Fossati-Jimack, *Ann Rheum Dis* **65**, 216 (Feb, 2006).
15. R. Hanayama *et al.*, *Science* **304**, 1147 (May 21, 2004).
16. M. Botto *et al.*, *Nat Genet* **19**, 56 (May, 1998).
17. E. Reefman *et al.*, *Arthritis Rheum* **56**, 3399 (Oct, 2007).
18. L. M. Stuart, K. Takahashi, L. Shi, J. Savill, R. A. Ezekowitz, *J Immunol* **174**, 3220 (Mar 15, 2005).
19. A. Devitt *et al.*, *J Cell Biol* **167**, 1161 (Dec 20, 2004).
20. N. Araki, M. T. Johnson, J. A. Swanson, *J Cell Biol* **135**, 1249 (Dec, 1996).
21. D. Cox, C. C. Tseng, G. Bjekic, S. Greenberg, *J Biol Chem* **274**, 1240 (Jan 15, 1999).
22. F. Nimmerjahn, J. V. Ravetch, *Nat Rev Immunol* **8**, 34 (Jan, 2008).
23. A. Bergtold, D. D. Desai, A. Gavhane, R. Clynes, *Immunity* **23**, 503 (Nov, 2005).

24. C. Bonnerot *et al.*, *EMBO J* **17**, 4606 (Aug 17, 1998).

25. R. G. Bredius *et al.*, *Immunology* **83**, 624 (Dec, 1994).

26. D. Cox, B. M. Dale, M. Kashiwada, C. D. Helgason, S. Greenberg, *J Exp Med* **193**, 61 (Jan 1, 2001).

27. M. J. Rauh, G. Krystal, *Clin Invest Med* **25**, 68 (Jun, 2002).

28. S. Bolland, J. V. Ravetch, *Immunity* **13**, 277 (Aug, 2000).

29. M. C. Blank *et al.*, *Hum Genet* **117**, 220 (Jul, 2005).

30. Y. Jiang *et al.*, *Int Immunol* **11**, 1685 (Oct, 1999).

31. K. Matsumoto *et al.*, *Arthritis Rheum* **48**, 486 (Feb, 2003).

32. R. Clynes, C. Dumitru, J. V. Ravetch, *Science* **279**, 1052 (Feb 13, 1998).

33. N. Barnes *et al.*, *Immunity* **16**, 379 (Mar, 2002).

34. M. Daeron, *Annu Rev Immunol* **15**, 203 (1997).

35. M. D. Hulett, P. M. Hogarth, *Mol Immunol* **35**, 989 (Oct, 1998).

36. L. Bevaart *et al.*, *Cancer Res* **66**, 1261 (Feb 1, 2006).

37. S. R. Lee *et al.*, *J Immunol* **189**, 3859 (Oct 15, 2012).

38. Z. Y. Huang *et al.*, *J Leukoc Biol* **80**, 1553 (Dec, 2006).

39. J. W. Booth, M. K. Kim, A. Jankowski, A. D. Schreiber, S. Grinstein, *EMBO J* **21**, 251 (Feb 1, 2002).

40. M. T. Crowley *et al.*, *J Exp Med* **186**, 1027 (Oct 6, 1997).

41. B. M. Dale, D. Traum, H. Erdjument-Bromage, P. Tempst, S. Greenberg, *J Immunol* **182**, 5654 (May 1, 2009).

42. M. Kavai, K. Lukacs, I. Sonkoly, K. Paloczi, G. Szegedi, *Ann Rheum Dis* **38**, 79 (Feb, 1979).

43. M. Kavai, G. Szegedi, *Autoimmun Rev* **6**, 497 (Aug, 2007).

44. S. A. Wu *et al.*, *Lupus* **22**, 279 (Mar, 2013).

45. L. S. Mayorga, F. Bertini, P. D. Stahl, *J Biol Chem* **266**, 6511 (Apr 5, 1991).

46. C. Raiborg, H. Stenmark, *Nature* **458**, 445 (Mar 26, 2009).

47. P. S. Bilodeau, J. L. Urbanowski, S. C. Winistorfer, R. C. Piper, *Nat Cell Biol* **4**, 534 (Jul, 2002).

48. M. Babst, D. J. Katzmann, W. B. Snyder, B. Wendland, S. D. Emr, *Dev Cell* **3**, 283 (Aug, 2002).

49. D. J. Katzmann, M. Babst, S. D. Emr, *Cell* **106**, 145 (Jul 27, 2001).

50. M. Babst, D. J. Katzmann, E. J. Estepa-Sabal, T. Meerloo, S. D. Emr, *Dev Cell* **3**, 271 (Aug, 2002).

51. C. Alvarez-Dominguez, A. M. Barbieri, W. Beron, A. Wandinger-Ness, P. D. Stahl, *J Biol Chem* **271**, 13834 (Jun 7, 1996).

52. R. A. Fratti, J. M. Backer, J. Gruenberg, S. Corvera, V. Deretic, *J Cell Biol* **154**, 631 (Aug 6, 2001).

53. O. V. Vieira *et al.*, *Mol Cell Biol* **23**, 2501 (Apr, 2003).

54. D. Poteryaev, S. Datta, K. Ackema, M. Zerial, A. Spang, *Cell* **141**, 497 (Apr 30, 2010).

55. J. Rink, E. Ghigo, Y. Kalaidzidis, M. Zerial, *Cell* **122**, 735 (Sep 9, 2005).

56. L. E. Via *et al.*, *J Biol Chem* **272**, 13326 (May 16, 1997).

57. E. A. Roberts, J. Chua, G. B. Kyei, V. Deretic, *J Cell Biol* **174**, 923 (Sep 25, 2006).

58. R. E. Harrison, C. Bucci, O. V. Vieira, T. A. Schroer, S. Grinstein, *Mol Cell Biol* **23**, 6494 (Sep, 2003).

59. D. R. Fernandez *et al.*, *J Immunol* **182**, 2063 (Feb 15, 2009).

60. R. Marini, A. Condino-Neto, S. Appenzeller, A. M. Morcillo, L. T. Costallat, *Rheumatol Int* **32**, 1977 (Jul, 2012).

61. V. Brinkmann *et al.*, *Science* **303**, 1532 (Mar 5, 2004).

62. T. A. Fuchs *et al.*, *J Cell Biol* **176**, 231 (Jan 15, 2007).

63. M. von Kockritz-Blickwede *et al.*, *Blood* **111**, 3070 (Mar 15, 2008).

64. C. C. Mihalache *et al.*, *J Immunol* **186**, 6532 (Jun 1, 2011).

65. G. S. Garcia-Romo *et al.*, *Sci Transl Med* **3**, 73ra20 (Mar 9, 2011).

66. R. Lande *et al.*, *Sci Transl Med* **3**, 73ra19 (Mar 9, 2011).

67. A. Hakkim *et al.*, *Proc Natl Acad Sci U S A* **107**, 9813 (May 25, 2010).

68. E. Villanueva *et al.*, *J Immunol* **187**, 538 (Jul 1, 2011).

69. A. M. Campbell, M. Kashgarian, M. J. Shlomchik, *Sci Transl Med* **4**, 157ra141 (Oct 24, 2012).

70. C. M. Cale, L. Morton, D. Goldblatt, *Clin Exp Immunol* **148**, 79 (Apr, 2007).

71. S. Manzi *et al.*, *Arthritis Rheum* **34**, 101 (Jan, 1991).

72. J. Schaller, *Ann Intern Med* **76**, 747 (May, 1972).

73. R. S. Flannagan, G. Cosio, S. Grinstein, *Nat Rev Microbiol* **7**, 355 (May, 2009).

74. M. Gaszner, A. Udvardy, *Biochem Biophys Res Commun* **181**, 44 (Nov 27, 1991).

75. A. Hasilik, K. von Figura, E. Conzelmann, H. Nehrkorn, K. Sandhoff, *Eur J Biochem* **125**, 317 (Jul, 1982).

76. A. R. Mantegazza *et al.*, *Blood* **112**, 4712 (Dec 1, 2008).

77. A. Savina *et al.*, *Cell* **126**, 205 (Jul 14, 2006).

78. A. Savina *et al.*, *Immunity* **30**, 544 (Apr 17, 2009).

79. L. Delamarre, M. Pack, H. Chang, I. Mellman, E. S. Trombetta, *Science* **307**, 1630 (Mar 11, 2005).

80. A. M. Lennon-Dumenil *et al.*, *J Exp Med* **196**, 529 (Aug 19, 2002).

81. R. M. Steinman, J. Swanson, *J Exp Med* **182**, 283 (Aug 1, 1995).

82. J. M. Rybicka, D. R. Balce, M. F. Khan, R. M. Krohn, R. M. Yates, *Proc Natl Acad Sci U S A* **107**, 10496 (Jun 8, 2010).

83. M. Kavai, I. Csipo, I. Sonkoly, J. Csongor, G. Y. Szegedi, *Scand J Immunol* **24**, 527 (Nov, 1986).

84. L. I. Matul'skaia, V. Klimov, T. A. Riazantseva, G. N. Pleskovskaia, *Vopr Med Khim* **32**, 32 (Jan-Feb, 1986).

85. H. D. Shin *et al.*, *J Hum Genet* **50**, 107 (2005).

86. R. F. Holcombe *et al.*, *Lupus* **3**, 97 (Apr, 1994).

87. K. Kannan *et al.*, *Cell Immunol* **171**, 10 (Jul 10, 1996).

88. S. R. Christensen *et al.*, *Immunity* **25**, 417 (Sep, 2006).

89. C. M. Lau *et al.*, *J Exp Med* **202**, 1171 (Nov 7, 2005).

90. E. A. Leadbetter *et al.*, *Nature* **416**, 603 (Apr 11, 2002).

91. K. M. Nickerson *et al.*, *J Immunol* **184**, 1840 (Feb 15, 2010).

92. G. A. Viglianti *et al.*, *Immunity* **19**, 837 (Dec, 2003).

93. M. M. Brinkmann *et al.*, *J Cell Biol* **177**, 265 (Apr 23, 2007).

94. S. E. Ewald *et al.*, *Nature* **456**, 658 (Dec 4, 2008).

95. Y. M. Kim, M. M. Brinkmann, M. E. Paquet, H. L. Ploegh, *Nature* **452**, 234 (Mar 13, 2008).

96. B. L. Lee *et al.*, *Elife* **2**, e00291 (2013).

97. B. Park *et al.*, *Nat Immunol* **9**, 1407 (Dec, 2008).

98. J. A. Deane *et al.*, *Immunity* **27**, 801 (Nov, 2007).

99. P. Pisitkun *et al.*, *Science* **312**, 1669 (Jun 16, 2006).

100. S. Subramanian *et al.*, *Proc Natl Acad Sci U S A* **103**, 9970 (Jun 27, 2006).

101. S. J. Rozzo *et al.*, *Immunity* **15**, 435 (Sep, 2001).

102. T. L. Roberts *et al.*, *Science* **323**, 1057 (Feb 20, 2009).

103. R. Panchanathan *et al.*, *J Immunol* **186**, 6762 (Jun 15, 2011).

104. Q. Yin *et al.*, *Cell Rep* **4**, 327 (Jul 25, 2013).

105. M. Lech *et al.*, *Ann Rheum Dis* (Aug 18, 2014).

106. C. A. Yang, S. T. Huang, B. L. Chiang, *Rheumatology (Oxford)* **54**, 324 (Feb, 2015).

107. Q. Yang *et al.*, *J Rheumatol* **41**, 444 (Mar, 2014).

108. J. Zhao *et al.*, *Arthritis Rheum* **65**, 3176 (Dec, 2013).

109. J. Ahn, D. Gutman, S. Saijo, G. N. Barber, *Proc Natl Acad Sci U S A* **109**, 19386 (Nov 20, 2012).

110. G. Dong *et al.*, *Mol Cells* (May 7, 2015).

111. J. Klarquist *et al.*, *J Immunol* **193**, 6124 (Dec 15, 2014).

112. S. Sharma *et al.*, *Proc Natl Acad Sci U S A* **112**, E710 (Feb 17, 2015).

113. D. A. Rhodes, J. Trowsdale, *Mol Immunol* **44**, 2406 (Mar, 2007).

114. W. A. McEwan *et al.*, *Nat Immunol* **14**, 327 (Apr, 2013).

115. K. Yang *et al.*, *J Immunol* **182**, 3782 (Mar 15, 2009).

116. M. Dugar, S. Cox, V. Limaye, T. P. Gordon, P. J. Roberts-Thomson, *Postgrad Med J* **86**, 79 (Feb, 2010).

117. F. J. Lopez-Longo *et al.*, *J Rheumatol* **21**, 1450 (Aug, 1994).

118. I. Peene, L. Meheus, E. M. Veys, F. De Keyser, *Ann Rheum Dis* **61**, 1090 (Dec, 2002).

119. M. B. Frank *et al.*, *Am J Hum Genet* **52**, 183 (Jan, 1993).

120. V. Oke *et al.*, *J Invest Dermatol* **129**, 2000 (Aug, 2009).

121. P. A. Lyons *et al.*, *Ann Rheum Dis* **69**, 1208 (Jun, 2010).

122. D. Ferrari *et al.*, *J Immunol* **176**, 3877 (Apr 1, 2006).

123. J. M. Labasi *et al.*, *J Immunol* **168**, 6436 (Jun 15, 2002).

124. M. Solle *et al.*, *J Biol Chem* **276**, 125 (Jan 5, 2001).

125. S. Adriouch *et al.*, *J Immunol* **169**, 4108 (Oct 15, 2002).

126. R. Auger, I. Motta, K. Benihoud, D. M. Ojcius, J. M. Kanellopoulos, *J Biol Chem* **280**, 28142 (Jul 29, 2005).

127. C. Virginio, A. MacKenzie, R. A. North, A. Surprenant, *J Physiol* **519 Pt 2**, 335 (Sep 1, 1999).

128. S. M. Le Gall *et al.*, *PLoS One* **7**, e52161 (2012).

129. M. Jindrichova *et al.*, *J Neurochem* (Feb 23, 2015).

130. S. K. Nath *et al.*, *Am J Hum Genet* **74**, 73 (Jan, 2004).

131. G. M. Chen *et al.*, *Mutagenesis* **28**, 351 (May, 2013).

132. K. Elkon, P. Casali, *Nat Clin Pract Rheumatol* **4**, 491 (Sep, 2008).

133. I. K. Poon, C. D. Lucas, A. G. Rossi, K. S. Ravichandran, *Nat Rev Immunol* **14**, 166 (Mar, 2014).

134. L. Ronnblom, V. Pascual, *Lupus* **17**, 394 (May, 2008).

135. M. W. Boule *et al.*, *J Exp Med* **199**, 1631 (Jun 21, 2004).

136. B. A. O'Brien, W. E. Fieldus, C. J. Field, D. T. Finegood, *Cell Death Differ* **9**, 457 (Apr, 2002).

137. T. Nakajima *et al.*, *Arthritis Rheum* **38**, 485 (Apr, 1995).

138. M. Bijl, E. Reefman, G. Horst, P. C. Limburg, C. G. Kallenberg, *Ann Rheum Dis* **65**, 57 (Jan, 2006).

139. M. Fischbach, *J Immunol* **133**, 2365 (Nov, 1984).

140. J. Yan, B. P. Harvey, R. J. Gee, M. J. Shlomchik, M. J. Mamula, *J Immunol* **177**, 4481 (Oct 1, 2006).

141. A. Kirisits, D. Pils, M. Krainer, *Int J Biochem Cell Biol* **39**, 2173 (2007).

142. M. Sharma *et al.*, *J Cell Biol* **164**, 923 (Mar 15, 2004).

143. P. S. Manzanillo, M. U. Shiloh, D. A. Portnoy, J. S. Cox, *Cell Host Microbe* **11**, 469 (May 17, 2012).

144. A. J. Perrin, X. Jiang, C. L. Birmingham, N. S. So, J. H. Brumell, *Curr Biol* **14**, 806 (May 4, 2004).

145. L. Marnell, C. Mold, T. W. Du Clos, *Clin Immunol* **117**, 104 (Nov, 2005).

146. D. L. Mallery *et al.*, *Proc Natl Acad Sci U S A* **107**, 19985 (Nov 16, 2010).

147. A. Kuznik *et al.*, *J Immunol* **186**, 4794 (Apr 15, 2011).

148. T. Kawai *et al.*, *Nat Immunol* **5**, 1061 (Oct, 2004).

149. C. Gunther *et al.*, *J Clin Invest* **125**, 413 (Jan, 2015).

150. M. Napirei *et al.*, *Nat Genet* **25**, 177 (Jun, 2000).

151. D. Skiljevic *et al.*, *Clin Chem Lab Med* **51**, 1083 (May, 2013).

152. M. A. Lee-Kirsch *et al.*, *Nat Genet* **39**, 1065 (Sep, 2007).

153. Y. Ren *et al.*, *Arthritis Rheum* **48**, 2888 (Oct, 2003).

154. J. C. Cambier, S. B. Gauld, K. T. Merrell, B. J. Vilen, *Nat Rev Immunol* **7**, 633 (Aug, 2007).

155. S. M. Anderson, M. M. Tomayko, M. J. Shlomchik, *Immunol Rev* **211**, 280 (Jun, 2006).

156. I. N. Bruce, M. B. Urowitz, D. D. Gladman, D. Ibanez, G. Steiner, *Arthritis Rheum* **48**, 3159 (Nov, 2003).

157. L. Iaccarino *et al.*, *Autoimmun Rev* **12**, 363 (Jan, 2013).

158. M. D. Lockshin, A. B. Levine, D. Erkan, *Lupus Sci Med* **2**, e000084 (2015).

159. J. H. Cho, M. Feldman, *Nat Med* **21**, 730 (Jul, 2015).

160. E. F. Remmers *et al.*, *N Engl J Med* **357**, 977 (Sep 6, 2007).

161. P. S. Ramos *et al.*, *PLoS Genet* **7**, e1002406 (Dec, 2011).

162. U. H. Rudofsky, B. D. Evans, S. L. Balaban, V. D. Mottironi, A. E. Gabrielsen, *Lab Invest* **68**, 419 (Apr, 1993).

163. C. Jiang *et al.*, *J Immunol* **178**, 7422 (Jun 1, 2007).

164. V. Kouskoff *et al.*, *Cell* **87**, 811 (Nov 29, 1996).

165. B. C. Schaefer, M. L. Schaefer, J. W. Kappler, P. Marrack, R. M. Kedl, *Cell Immunol* **214**, 110 (Dec 15, 2001).

166. R. H. Valdivia, S. Falkow, *Science* **277**, 2007 (Sep 26, 1997).

167. J. Hua, K. Kirou, C. Lee, M. K. Crow, *Arthritis Rheum* **54**, 1906 (Jun, 2006).

168. H. Appelqvist, P. Waster, K. Kagedal, K. Ollinger, *J Mol Cell Biol* **5**, 214 (Aug, 2013).

169. A. Monteith *et al.*, *PLoS One* **8**, e58059 (2013).

170. D. Fernandez, A. Perl, *Autoimmun Rev* **8**, 184 (Jan, 2009).

171. D. Fernandez, A. Perl, *Discov Med* **9**, 173 (Mar, 2010).

172. P. B. Dennis *et al.*, *Science* **294**, 1102 (Nov 2, 2001).

173. K. Huang, D. C. Fingar, *Semin Cell Dev Biol* **36**, 79 (Dec, 2014).

174. C. C. Thoreen *et al.*, *J Biol Chem* **284**, 8023 (Mar 20, 2009).

175. Y. Sancak *et al.*, *Cell* **141**, 290 (Apr 16, 2010).

176. E. Jacinto *et al.*, *Nat Cell Biol* **6**, 1122 (Nov, 2004).

177. D. D. Sarbassov *et al.*, *Curr Biol* **14**, 1296 (Jul 27, 2004).

178. T. S. Gomez, J. A. Gorman, A. A. de Narvajas, A. O. Koenig, D. D. Billadeau, *Mol Biol Cell* **23**, 3215 (Aug, 2012).

179. J. S. King *et al.*, *Mol Biol Cell* **24**, 2714 (Sep, 2013).

180. K. Zheng, K. Kitazato, Y. Wang, Z. He, *Crit Rev Microbiol*, 1 (Apr 8, 2015).

181. S. Arber *et al.*, *Nature* **393**, 805 (Jun 25, 1998).

182. N. Yang *et al.*, *Nature* **393**, 809 (Jun 25, 1998).

183. S. Shalini, L. Dorstyn, S. Dawar, S. Kumar, *Cell Death Differ* **22**, 526 (Apr, 2015).

184. J. Li *et al.*, *Nat Cell Biol* **9**, 276 (Mar, 2007).

185. A. Akhter *et al.*, *Immunity* **37**, 35 (Jul 27, 2012).

186. A. Sokolovska *et al.*, *Nat Immunol* **14**, 543 (Jun, 2013).

187. S. Wang *et al.*, *Cell* **92**, 501 (Feb 20, 1998).

188. S. Seto, K. Tsujimura, Y. Koide, *Nihon Rinsho* **69**, 1373 (Aug, 2011).

189. C. E. Becker, E. M. Creagh, L. A. O'Neill, *J Biol Chem* **284**, 34531 (Dec 11, 2009).

190. R. M. Siegel, *Nat Rev Immunol* **6**, 308 (Apr, 2006).

191. N. Kayagaki *et al.*, *Nature* (Sep 16, 2015).

192. J. Shi *et al.*, *Nature* (Sep 16, 2015).

193. E. A. Miao, J. V. Rajan, A. Aderem, *Immunol Rev* **243**, 206 (Sep, 2011).

194. Y. Aachoui *et al.*, *Science* **339**, 975 (Feb 22, 2013).

195. K. Kuida *et al.*, *Science* **267**, 2000 (Mar 31, 1995).

196. N. Kayagaki *et al.*, *Nature* **479**, 117 (Nov 3, 2011).

197. S. Mariathasan *et al.*, *Nature* **430**, 213 (Jul 8, 2004).

198. E. S. Lander, *Science* **274**, 536 (Oct 25, 1996).

199. N. Risch, K. Merikangas, *Science* **273**, 1516 (Sep 13, 1996).

200. D. S. Cunninghame Graham, M. Akil, T. J. Vyse, *Rheumatology (Oxford)* **46**, 927 (Jun, 2007).

201. D. S. Cunninghame Graham *et al.*, *Genes Immun* **9**, 93 (Mar, 2008).

202. R. R. Graham *et al.*, *Nat Genet* **40**, 1059 (Sep, 2008).

203. G. Hom *et al.*, *N Engl J Med* **358**, 900 (Feb 28, 2008).

204. G. International Consortium for Systemic Lupus Erythematosus *et al.*, *Nat Genet* **40**, 204 (Feb, 2008).

205. S. Kobayashi *et al.*, *Arthritis Rheum* **58**, 1940 (Jul, 2008).

206. S. V. Kozyrev *et al.*, *Nat Genet* **40**, 211 (Feb, 2008).

207. S. K. Nath *et al.*, *Nat Genet* **40**, 152 (Feb, 2008).

208. R. J. Palomino-Morales *et al.*, *Genes Immun* **9**, 379 (Jun, 2008).

209. A. H. Sawalha *et al.*, *PLoS One* **3**, e1727 (2008).

210. S. Sigurdsson *et al.*, *Hum Mol Genet* **17**, 2868 (Sep 15, 2008).

211. S. Sigurdsson *et al.*, *Am J Hum Genet* **76**, 528 (Mar, 2005).

212. K. E. Taylor *et al.*, *PLoS Genet* **4**, e1000084 (May, 2008).

213. P. M. Visscher, M. A. Brown, M. I. McCarthy, J. Yang, *Am J Hum Genet* **90**, 7 (Jan 13, 2012).

214. G. M. Barton, J. C. Kagan, *Nat Rev Immunol* **9**, 535 (Aug, 2009).

215. K. Nundel *et al.*, *J Immunol* **194**, 2504 (Mar 15, 2015).

216. J. F. Huang *et al.*, *Science* **286**, 952 (Oct 29, 1999).

217. D. Hudrisier, J. Riond, H. Mazarguil, J. E. Gairin, E. Joly, *J Immunol* **166**, 3645 (Mar 15, 2001).

218. I. Hwang *et al.*, *J Exp Med* **191**, 1137 (Apr 3, 2000).

219. D. G. Osborne, S. A. Wetzel, *J Immunol* **189**, 4728 (Nov 15, 2012).

220. S. A. Wetzel, T. W. McKeithan, D. C. Parker, *J Immunol* **174**, 80 (Jan 1, 2005).

221. S. Daubeuf *et al.*, *Immunol Invest* **36**, 687 (2007).

222. A. L. Puaux *et al.*, *Eur J Immunol* **36**, 779 (Mar, 2006).

223. S. Pfirsch-Maisonnas *et al.*, *Sci Signal* **4**, ra24 (2011).